Noble gases in Dome C micrometeorites - An attempt to disentangle asteroidal and cometary sources

Bastian Baecker, Ulrich Ott, Mario Trieloff, Cécile Engrand, Jean Duprat

Noble gases in Dome C micrometeorites - an attempt to disentangle asteroidal and cometary sources

Bastian Baecker[1,2†], Ulrich Ott[1,2,3*], Mario Trieloff[2],
Cécile Engrand[4], and Jean Duprat[5]

[1]Max-Planck Institut für Chemie, Hahn-Meitner-Weg 1, 55128 Mainz, Germany
[2]Klaus-Tschira-Labor für Kosmochemie, Institut für Geowissenschaften, Universität Heidelberg, Im Neuenheimer Feld 234-236, 69120 Heidelberg, Germany
[3]MTA Atomki, Bem tér 18/C, 4026 Debrecen, Hungary
[4]IJCLab, CNRS-Paris-Saclay, Orsay, France
[5]IMPMC, CNRS-MNHN, Paris, France

*corresponding author; e-mail: uli.ott@mpic.de; phone: +49-6136-42609
[†]current address: Elbeallee 51, 14612 Falkensee, Germany

Abstract

We have performed a comprehensive noble gas study, including the isotopes of krypton and xenon, on a set of micrometeorites (MMs) collected from surface snow at Dome C (DC) on the Antarctic plateau. He and Ne are generally dominated by a solar component, with lower ^{4}He concentrations and ^{4}He/^{20}Ne ratios in crystalline (Xtal) compared to fine-grained carbonaceous (FgC) MMs. Concentrations of (surface-correlated) solar wind (SW) He and Ne in FgC MMs are at the high end of what has been seen in earlier work, whereas the abundances of (volume-correlated) Kr and Xe are similar to what has been found in previous studies of MMs. In most samples, isotopic ratios for Kr and Xe are in the usual range of Q-Kr and -Xe (the Q component is the dominating component in primitive macroscopic meteorites) and air. When quantifiable, cosmic ray exposure (CRE) ages based on cosmogenic ^{21}Ne and ^{3}He, in combination with the Poynting-Robertson effect, are broadly consistent with an origin of the MMs from the asteroid belt. An exception is an Xtal MM, which exhibits a cosmogenic ^{21}Ne concentration in agreement with an origin from beyond Saturn, consistent with a possible cometary origin. In addition, data for trapped noble gases in three (out of ten analyzed) DC MMs provide hints that these may be related to a cometary source. One sample, a fragment of a FgC MM, is of particular interest. This fragment exhibits a Xe composition, although with large analytical uncertainties, deficient in the heavy isotopes ^{134}Xe and ^{136}Xe. This is similar to the Xe isotopic pattern, probably related to cometary ice, measured by Rosetta in the coma of comet 67P/Churyumov-Gerasimenko. The same MM also has an unusually high ^{36}Ar/^{38}Ar ratio, consistent with Rosetta's Ar measurement (in this case the latter having a large uncertainty). The other hints are for two MMs, of crystalline (Xtal) type, that show Ne similar to that found in laboratory analysis of refractory grains captured from comet 81P/Wild 2 by the Stardust mission. Additionally, a FgC/Xtal MM may contain excess ^{3}He, similar to what has been seen in some cluster interplanetary dust particles (cluster IDPs).

Keywords: micrometeorites; noble gases; cosmic ray exposure; comets; asteroids

1. Introduction

The study of noble gases (and other volatiles) in micrometeorites is of interest for various reasons. One concerns the origin and evolution of the atmospheres of Earth and other inner solar system rocky planets, which is one of the outstanding questions in planetology. A variety of processes contributing the volatiles H, C, N and noble gases have been considered (e.g., Maurette et al., 2000; Trieloff et al., 2000; Pepin and Porcelli, 2002; Marty, 2012; Alexander et al., 2012; Albarède et al., 2013; Vogt et al., 2019; and references therein), including the possibility of accretion of volatile-rich materials by the forming planets. This infalling material may have been in form of planetesimals and/or interplanetary dust grains, from the outer asteroid belt, as well as cometary material from the outer solar system (Pepin, 2006; Marty, 2012; Bradley et al., 2014). Recent models for the origin of Earth's atmosphere favor the contribution of a few percent of volatile-rich material, similar to carbonaceous chondrites, accounting for the bulk of the volatile inventory (Marty, 2012; Albarède et al., 2013), but the timing of such contribution is still a matter of debate. Some contribution from comets appears to be required based on recent analyses of volatiles in the coma of the Jupiter family comet (JFC) 67P/Churyumov-Gerasimenko (Marty et al., 2016, 2017).

Generally, one might expect that the contribution to the geochemical budget of the planets arising from infalling dust and planetesimals might be similar in composition to that from primitive meteorites. In fact, Marty (2012) proposes that the isotopic compositions of H, N, Ne and Ar of Earth's reservoirs can be explained by mixing of solar and chondritic end-members, with cometary contributions limited to a few percent. This was recently revisited with a model proposing an accretion of the Earth from enstatite-chondrite-like composition, with the need of later delivery of volatiles from an exogeneous source to account for the isotopic composition of the ocean water (Piani et al., 2020). However, "classical", i.e. macroscopic chondritic meteorites (i.e., with sizes in the range centimeter to meters) provide only a small contribution to the influx of extraterrestrial material to Earth, at least over the recent geological time scale. Instead, the dominant source of extraterrestrial material accreted by the Earth today is represented by micrometeorites (MMs) with sizes less than a mm (Love and Brownlee, 1993; Cremonese et al., 2012; Carrilo-Sánchez et al., 2020, Rojas et al., 2021). Such MMs can be recovered from polar ice and snow from Greenland and Antarctica (Maurette et al., 1991; Maurette et al., 2000; Taylor et al., 2000; Duprat et al., 2007; Rochette et al., 2008; Genge et al., 2018). Estimates for the present flux of micrometeorites before atmospheric entry are based on the study of hypervelocity impact craters on the Long Duration Exposure Facility (LDEF) spacecraft. From these, Love and Brownlee (1993) derived a total mass influx accreted by Earth of 40 (± 20) x 10^6 kg per year, while a reevaluation of the LDEF data by Cremonese et al. (2012) suggests lower total mass influx rates, between 7.4 (± 1.0) and 4.2 (± 0.5) x 10^6 kg per year, the value depending on the assumed source - asteroidal or cometary. Estimates based on space observations and/or modelling have, among others, been published by Grün et al. (1985), Nesvorný et al. (2010) and, most recently, Carrillo-Sánchez et al. (2020). The latter yields a value of 10.2 x 10^6 kg per year, and also provides estimates for fluxes to Mars of 0.75 x 10^6 kg/year (surprisingly low in comparison to earlier estimates, e.g., Flynn, 1996) and for Venus of 11.3 x 10^6 kg/year, respectively.

During their high velocity impact at Earth's atmosphere during entry, a portion of interplanetary particles is fully vaporized, while the remaining part survives as melted, partly melted and unmelted particles. Using Lidar observations of the vertical flux of mesospheric Na (originating from the vaporized part), Gardner et al. (2014) inferred an intermediate influx value (see this paper also for further estimates given in the literature). The fraction of the flux that survives as particles reaching Earth's surface has been measured in various collections, mainly from Antarctica. Values of ~1.6 x 10^6 kg were obtained from the amount of cosmic spherules recovered from the South Pole Water well (Taylor et al., 2012) and Transantarctic Mountains (Suttle and Folco, 2020), where the latter corresponds to an average over a ~10^6 year timescale. A measurement of the recent flux was performed at Dome C, using the collection from which the particles studied in this paper come from, by Rojas et al. (2021). The accurate control on the exposure parameter S (expressed in m^2 times year) allowed to infer an annual flux of about 5 x 10^6 kg, summing both melted (i.e. cosmic spherules) and un-melted (uMMs) particles (Rojas et al, 2021).

Carrillo-Sánchez et al. (2020) combined a chemical ablation model (CABMOD) with a Zodiacal Cloud Model (Zody), which also allowed to obtain separate predictions for the contributions from different sources: asteroidal, Jupiter-family comets (JFC) and Halley-type comets (HTC). In case of Earth (and Mars), their model predicts, in agreement with previous studies (Nesvorný et al., 2010), the dominant flux to be in form of unmelted MMs, and the dominant source to be comets, not only for the most fine-grained dust, but also in the size range of the MMs (~200 μm diameter) that we studied in this work.

While MMs were initially mainly related to primitive CM-chondrite-like material based on mineralogical, chemical and isotopic studies, more diversity has become obvious as more micrometeorite collections were performed and extensively studied. A substantial fraction of the micrometeorite population (10 to 17%; Taylor et al., 2012; Cordier and Folco, 2014) may be similar to ordinary chondrites and related to asteroids (Genge, 2008; Cordier et al., 2011a; Suavet et al., 2011; van Ginneken et al., 2012; Imae et al., 2013; Noguchi et al., 2015; Shyam Prasad et al., 2018), while a smaller fraction (less than 6%) has been linked to differentiated asteroids such as the Vestoids (Taylor et al., 2007; Cordier et al., 2011b, 2012). There is also a specific family of MMs, the so-called ultra-carbonaceous micrometeorites (UCAMMs), that has a probable cometary origin. These particles, which have extremely high concentrations of carbon (Dartois et al., 2018), have been identified in collections from both Concordia Station (Dome C; Duprat et al., 2010) and Dome Fuji Station (Nakamura et al., 2005; Noguchi et al., 2015), and a cometary origin is inferred from their large deuterium excesses (Duprat et al., 2010) and the high nitrogen content of their organic matter (Dartois et al., 2013; Yabuta et al., 2017). Apparently, the diversity of micrometeorites is large, and selection effects may play a role in the assessment (Genge et al., 2020), since larger MMs are more easily found on Earth and easier to study. In any case, in the size range of the MMs that we have studied (Table 1), there should be a fair chance to encounter cometary (in particular, JFC) particles (Rojas et al, 2021).

Based on an early set of data, Maurette et al. (2000) evaluated the possible contribution of micrometeorites to neon, organics, carbon dioxide, nitrogen and water on Earth and they

concluded that early accretion of primitive micrometeorites may have played a major role in the formation of the terrestrial atmosphere and oceans. In a more recent evaluation, Vogt et al. (2019) conclude that interplanetary particles (IDPs) and micrometeorites (MMs) may very well be an important source of Earth's neon (both interior and atmospheric). However, a crucial ingredient in these estimates is the pre-Archean micrometeorite flux that has to be extrapolated from the present-day flux with an uncertainty that is still a matter of debate.

Another aspect of noble gases in MMs is that they may possibly allow to distinguish between asteroidal and cometary sources, as the relative contribution of each source to dust entering the terrestrial atmosphere is still an open question. A difficulty, in this respect, is that Ne and He, in (unmelted) small particles that travelled through interplanetary space, are generally dominated by implanted solar wind components. This has been demonstrated in numerous studies, as, in fact, most studies of noble gases in MMs have concentrated on He and/or Ne only (see summary in Wieler, 2002a). Still, sometimes small excesses of ^{21}Ne of cosmogenic origin have been observed, which allow, in combination with the Poynting-Robertson effect (Wyatt and Whipple, 1950) estimating a cosmic ray exposure age and inferring the place of origin. Using this approach, Trappitsch and Leya (2013) have re-examined the data available at the time and found three MMs that may have come from orbital distances far beyond the asteroidal belt, i.e. of possible cometary origin. This is, provided all cosmic ray exposure happened while the MMs were travelling as small particles. However, as the authors note, it is difficult to rule out that much or even most of the exposure occurred in a parent body regolith instead.

Less ambiguous would be signatures of trapped noble gas components. In case of an IDP ("Manchanito") the isotopic composition of Ne has been found to resemble Q-Ne (where Q is the major host phase of Ar, Kr and Xe – though not of Ne – in primitive meteorites). Since cometary Ne measured in samples returned by the Stardust mission (Marty et al., 2008) also resembles Q-Ne in composition, this has been taken as an indication for a cometary origin of this particle (Ogliore et al., 2020). Compared to He and Ne, the situation may be more favorable for the heavier noble gases, in particular Xe. There are clear differences between the composition of the trapped (i.e., non-radiogenic, non-cosmogenic) noble gas component in meteorites and the atmospheres of Earth and Mars, the solar wind and, apparently, also cometary noble gas. Compared to solar abundance ratios, trapped noble gases in primitive meteorites (the "planetary" component) are characterized by an elemental abundance pattern strongly favoring the heavy over the light noble gases. Similarly, in comparison to terrestrial and Martian atmospheres, marked differences appear, in particular in the Kr/Xe ratio and the isotopic composition of Xe (see, e.g., discussions in Ott and Begemann, 1985; Pepin, 1991; Owen et al., 1992; Owen and Bar-Nun, 1993; Owen, 2008; Ott, 2014; Ott et al., 2019). These differences cannot be explained by simple mixing of "planetary" and solar noble gases, unless some additional processing is invoked (e.g., Hébrard and Marty, 2014). Of particular interest here is the isotopic composition of Xe measured by the Rosetta spacecraft in the coma of JFC 67/P Churyumov-Gerasimenko (Marty et al., 2017), which is characterized by a unique pattern exhibiting a spectacular relative deficit of the two heaviest isotopes, ^{134}Xe and ^{136}Xe, by roughly 30 and 60 %, respectively, compared to common components. Identification in a MM would be an indication that it originated from a

parent body similar to 67/P-CG, more telling than the presence of Q-Ne, which appears also in primitive meteorites. Evidence for cometary Xe on the Moon may have been seen by Bekaert et al. (2017) and Pernet-Fisher et al. (2020), but the situation is complicated by the presence of contaminating (terrestrial) air and solar wind Xe. Modeling the Xe isotopic composition these authors measured in lunar anorthosites required, in addition to solar wind and air, a contribution from a component deficient in the heavy isotopes of Xe, such as in cometary (coma) Xe. While the origin of this Xe is not clear, one possibility is that it was introduced by micrometeorite impacts. Still, it is important to realize that Rosetta and Stardust sampled different types of cometary reservoirs, in addition to sampling different comets. Xe in the cometary coma measured by Rosetta corresponds to that carried in ices (maybe primarily the CO_2 fraction; Rubin et al., 2018), while Q-Ne was measured in solids captured from the cometary coma in the aerogel targets of the Stardust mission.

Previous studies of MMs including Ar and/or Kr and Xe are rare, see Marty et al. (2002, 2005), Osawa and Nagao (2002a), Osawa et al. (2000, 2003a, b, 2010) and Okazaki et al. (2015). Among these, Osawa et al. (2003a, 2010) focused on cosmic spherules where noble gas abundances were close to blank level in most cases. For the isotopes of Kr and Xe, fairly precise data were obtained (in addition to data for He, Ne, Ar) by Sarda et al. (1991) on a single large (230 μg) micrometeorite. Other results for the isotopes of Kr and Xe are reported in Osawa et al. (2000) and Osawa and Nagao (2002a, b), whose data, however, do not include the isotopes lighter than ^{82}Kr and ^{129}Xe. More recently, a few micrometeorite analyses were included within an integrated study on Xe in Interplanetary Dust Particles by Spring (2014), using the Relax (Refrigerator Enhanced Laser Analyzer for Xenon) instrument at Manchester University (UK) (Gilmour et al., 1994; Crowther et al., 2008). Further results for Xe isotopes in a few large unmelted Antarctic Cap-Prudhomme micrometeorites (Maurette, 2006) were reported in an abstract by Olinger et al. (2013). In a previous study, we reported a full set of noble gas data in micrometeorites from the Transantarctic Mountains (Cordier et al., 2018; Baecker et al, 2018). These micrometeorites accumulated since about a million years ago (Rochette et al., 2008; Folco et al., 2008) and were relatively large (several hundred μm). Here we report new results on a set of recently fallen, i.e. recovered from surface snow, MMs from the Concordia collection (Duprat et al., 2007), with sizes of typically ~200 μm. We also include results for a single MM from Cap Prudhomme (Maurette et al., 1991; Kurat et al., 1994).

2. Experimental Procedures

2.1. Dome C samples

Except for the one MM from Cap Prudhomme (Kurat et al., 1994), the analyzed samples are part of the Concordia collection. They were collected at the Concordia station, a station jointly constructed by the French and Italian Polar Institutes, which is located at Dome C, about 3200 m above sea level on the Antarctic plateau, and about 1100 km from the coast of Adélie land. For details about the collection protocol see Duprat et al. (2007).

Before allocation for noble gas analysis, the MMs had been stored under vacuum conditions and had been handled in a clean room. During selection, the samples were observed under higher magnification (115 x) and sizes of the allocated specimens were determined using a stereo-microscope with a μm-scale as a reference. Roughly 1/3 of each (by volume) of a given MM was allocated for noble gas analysis at the Max-Planck-Institute for Chemistry (MPIC) in Mainz, while the remaining sample was kept at IJCLab (Orsay). The weights of the fragments for noble gas analysis were calculated using the approximate volume (assuming sphere or cone-head shape) and a density of ~2.1 g/cm^3, as appropriate for CM and CI chondrites (Britt and Consolmagno, 2003). After selection and size measurements, the samples were deposited between two glass slides and transported to the MPIC.

Table 1. Dome C (DC) and Cap Prudhomme (CP) MMs analyzed for noble gases.

particle	fragment #*	size [µm]	weight [µg]	class$
Dome C				
DC 06_07_213	PL 09_20 3 (1)	97 x 91	~ 1.1	Xtal
DC 06_08_01	PL06_09A 1	110 x 92	~ 1.4	Xtal
DC 06_09_11	PL 07_01A 11	137 x 111	~ 1.3	FgC/Sc
DC 06_09_50	PL 07_02B 2	141 x 134	~ 3.3	FgC
DC 06_09_57	PL07_02B 9 (1)	74 x 36	~ 0.15	FgC
DC 06_09_57	PL07_02B 9 (2)	19 x 18	~ 0.01	FgC
DC 06_09_63	PL07_02C 3	198 x 141	~ 3.3	FgC/Xtal
DC 06_09_141	PL07_04C 9 (1)	84 x 79	~ 0.7	Xtal
DC 06_09_149	PL07_05A 5 (1)	85 x 60	~ 0.3	Xtal
DC 06_09_189	PL07_06A 9	93 x 92	~ 1.0	FgC/Sc
Cap Prudhomme				
CP 9-1-1994	PL 10-109-D9	252 x 188	~ 6.2	Sc

*Material available for noble gas analysis often consisted of several fragments. Where not the complete material was used, the fragment number is given in parentheses. The approximate weight was calculated as described in the text.

$Xtal = crystalline; FgC = fine-grained carbonaceous; Sc = scoriaceous.

Table 1 gives basic information about the analyzed samples. The respective sample name for each Dome C sample consists of the following combination: DC (Dome C) 06 (year 2006) 09 (number of the nylon filter where the particle was selected from) 247 (number of particle). Each particle was fragmented in a dedicated glass holder labelled, e.g., PL07 (year)_02B (glass holder) 7 (hole position). The Cap Prudhomme (CP) sample has a similar code system. For the noble gas work, we concentrated on unmelted MMs since these are most likely to have retained original noble gas signatures. The classification in Table 1 follows Kurat et al. (1994), Engrand and Maurette (1998) and Genge et al. (2008): FgC = fine-grained carbonaceous, Xtal =crystalline (consisting of coarse-grained anhydrous minerals). Only the CP sample is scoriaceous, with two additional DC samples (DC 06_09_11 and DC 06_09_189) partly scoriaceous.

2.2. Noble gas analysis

Details of our procedures for noble gas analysis of MMs at MPIC, Mainz, are given in our reports on MMs from the Transantarctic Mountains (Baecker et al., 2018: Cordier et al. 2018) and in the PhD thesis of B. Baecker (Baecker, 2014). In short, in view of the expected low gas amounts, a newly dedicated system was set up at MPIC that differs from our conventional systems (e.g., Schwenzer et al., 2007; Cartwright et al., 2014) primarily by two features: a) Laser heating for gas extraction in order to minimize extraction blank; and b) a high sensitivity Noblesse noble gas mass spectrometer (Nu Instruments) with multiple ion counting (MIC; 8 channeltrons, plus a Faraday cup for larger signals) for simultaneous isotope measurements, which maximizes the number of detected ions. This system requires

cross-calibration of the detectors and (minor) correction for cross talk, as described in Baecker et al. (2018).

Gas extraction was accomplished by heating with a 30 Watt CO_2 IR laser system (MIR 10-30, New Wave Research), after which the released gases were cleaned using successive exposures to Zr-Al SAES getters. They were separated into He plus Ne, Ar, Kr and Xe fractions, respectively, using temperature-controlled activated charcoal, and sequentially admitted to the mass spectrometer for analysis. Full multi-ion collection (MIC) was used for Kr and Xe only, where, for Xe, we used a three-step measurement routine (Baecker, 2014; Baecker et al., 2018). In case of Ar, isotopes ^{36}Ar and ^{38}Ar were measured on the central channeltron (IC3), while ^{40}Ar was measured using the Faraday cup. Similarly, ^{4}He was mostly measured by Faraday detector, while the ^{3}He signal was detected on IC3. As for Ne, all isotopes of Ne as well as mass 18 (water, used for correction at ^{20}Ne) were measured using IC 3. Masses 40 and 44, which were also used for interference correction, were measured by MIC using IC0 and IC6.

The DC samples were measured following the measurement of the TAM MMs (Baecker et al., 2018), at which time extraction blanks had become lower and more stable. Including interfering non-noble gas contributions at the respective masses, they were, in cm^3 STP, approximately as follows: ^{3}He: 2×10^{-15}, ^{4}He: 6×10^{-12}, ^{20}Ne: 4×10^{-13}, ^{22}Ne: 7×10^{-14}, ^{36}Ar: 4×10^{-13}, ^{40}Ar: 1.0×10^{-10}, ^{84}Kr: 1×10^{-14} and ^{132}Xe: 3×10^{-15}.

Interference corrections were applied at mass 3 for interference from not fully resolved HD/H_3, at the Ne isotopes for $^{1}H_2{}^{18}O$ as well as doubly charged ^{40}Ar and CO_2, and at the Ar isotopes ^{36}Ar and ^{38}Ar for HCl and hydrocarbons. These corrections were generally minor. Sensitivity and instrumental mass discrimination were determined by intermittent analyses of a noble gas mixture (obtained from *Air Liquide)* with atmospheric isotopic composition, to which extra ^{3}He had been added resulting in ^{3}He/^{4}He ~5×10^{-4}. Errors in all the corrections are included in the reported (1σ) uncertainties.

3. Results

3.1. Helium and neon

The results for He and Ne are reported in Tables 2 and 3. Similar as in previous micrometeorite studies, the abundances of the major isotopes ^{4}He and ^{20}Ne are dominated by solar wind. No helium was detected in the two fragments of DC 06_09_57, while in two cases (DC 06_09_141 and DC 06_09_189) we found ^{4}He, but ^{3}He was indistinguishable from background. The data for those MMs, where both isotopes were detected, are displayed in Fig. 1, a plot of ^{3}He/^{4}He in 10^{-4} units versus ^{4}He in cm^3 STP/g, alongside with the results from previous studies and reference compositions (see figure caption for references). Separately shown are the data from our previous analyses of the (larger) TAM MMs (Baecker et al., 2018; Cordier et al., 2018) and the (smaller) IDP Manzanito of Ogliore et al. (2020), which is of interest in the later discussion (chapter 4.5).

The isotopic ratios are broadly similar to previous studies, and also concentrations are within the range previously observed. Again, as noted before, solar wind He is present not only in unmelted MMs but also in such that have been partially molten (Sc = scoriaceous). Interestingly, there is a clear distinction between Dome C MMs that are classified as Xtal (crystalline) and others classified as FgC (= fine grained), FgC/Sc and FgC/Xtal. The highest ^{4}He concentrations are those of DC 06_09_189 (FgC/Sc) followed by DC 06_09_50 (FgC) and DC 06_09_63 (FgC/Xtal), which are among the highest reported so far. Not surprisingly, Xtal MMs with low ^{4}He concentrations show high ^{3}He/^{4}He ratios, distinctly higher than in all the trapped components shown, which is a clear indication for the presence of cosmogenic ^{3}He sited more retentively (volume-correlated) than solar wind He (surface-correlated). Conversely, the more gas-rich samples show ^{3}He/^{4}He ratios similar to the trapped components expected to be present, and it is difficult to assess the presence of cosmogenic He in these cases. An exception may be FgC/Xtal DC 06_09_63, where the ratio is only slightly below that of unfractionated trapped solar wind (see chapters 3.4 and 4.4).

The results for Ne are presented in Table 3. For the two fragments from DC 06_09_57, we obtained only upper limits, otherwise amounts of ^{22}Ne for the DC MMs range between ~5 x 10^{-13} cm^{3} STP and ~4 x 10^{-12} cm^{3} STP (concentrations between ~3 x 10^{-7} cm^{3} STP/g and ~7 x 10^{-6} cm^{3} STP/g). The scoriaceous MM from Cap Prudhomme is lower (2 x 10^{-13} cm^{3} STP and 3 x 10^{-8} cm^{3} STP/g, resp.). Isotopic ^{20}Ne/^{22}Ne ratios are >11, which clearly indicates substantial to dominant contributions from solar wind (SW and/or FSW). This is graphically shown in the three-isotope plot of Fig. 2. Fig. 2a compares our DC and CP data with previous results for MMs (see Figure Caption for references). Like for most of the previous studies, the data points plot roughly in the region between unfractionated solar wind (SW) and other trapped components with lower ^{20}Ne/^{22}Ne (Ne-B, fractionated solar wind = FSW, Q, EA). Contributions from cosmogenic Ne are small and difficult to establish precisely, if at all (chapters 3.4 and 4.4). Again, this is typical for most MMs. Only in a few cases, in particular for the scoriaceous MMs with low concentrations of solar Ne in our earlier TAM MM study (Baecker et al., 2018; Cordier et al, 2018), a clear shift to higher ^{21}Ne/^{22}Ne has been observed.

316 Table 2. He results for 10 different DC MM samples from 9 different MMs; as well as an additional
317 MM from Cap Prudhomme. Uncertainties in the last digits (1σ) are shown in parentheses and do not
318 include errors in sample weight. Where upper limits are listed, these are 2σ. For comparison, the
319 isotopic compositions of solar wind (SW), "fractionated solar wind" (FSW), Earth atmosphere (EA)
320 and the primordial components Q (P1) and HL are listed at the bottom.

Sample	**particle #**	**^{3}He** (10^{-14} cm^3 STP)	**^{4}He** (10^{-12} cm^3 STP)	**^{3}He** (10^{-8} cm^3 STP/g)	**^{4}He** (10^{-6} cm^3 STP/g)	**^{3}He/^{4}He** (10^{-4})
DC 06_07_213	PL 09_20 3 (1)	1.3 (3)	16.2 (3.9)	1.22 (28)	15.2 (3.7)	7.96 (2.76)
DC 06_08_01	PL06_09A 1	2.8 (3)	19.5 (3.9)	2.01 (27)	14.2 (3.0)	14.1 (3.3)
DC 06_09_11	PL 07_01A 11	2.8 (6)	86.7 (4.2)	2.13 (46)	67.1 (3.3)	3.18 (71)
DC 06_09_50	PL 07_02B 2	363 (15)	12150 (188)	109.9 (4.6)	3682 (57)	2.98 (12)
DC 06_09_57	PL07_02B 9 (1)	< 0.5	< 10	< 3.6	< 64	--
DC 06_09_57	PL07_02B 9 (2)	--	< 9	--	< 1141	--
DC 06_09_63	PL07_02C 3	131 (10)	3152 (57)	39.6 (2.9)	955 (17)	4.14 (30)
DC 06_09_141	PL07_04C 9 (1)	--	8.7 (4.3)	--	12.4 (6.1)	--
DC 06_09_149	PL07_05A 5 (1)	--	47.9 (4.3)	--	160 (14)	--
DC 06_09_189	PL07_06A 9	156 (3)	4799 (68)	156.3 (3.2)	4799 (68)	3.26 (9)
CP 9-1-1994	PL 10-109-D9	< 3.2	8.86 (5.67)	< 0.52	1.4 (9)	--

Component	**References**	**^{3}He/^{4}He** (10^{-4})
SW	[1]	4.645 (8)
"FSW"	[2], [3]	2.17 (5)
Q (P1)	[4]	1.23 (2)
EA	[5]	0.0140 (1)
HL	[6]	1.70 (10)

321 References: [1] Heber et al. (2012); [2] Benkert et al. (1993); [3] Wieler (2002a); [4] Busemann et al. (2000); [5] Ozima and Podosek
322 (2002); [6] Huss and Lewis (1994); Note: For more information regarding **"**FSW**"** see Wieler et al. (2007).

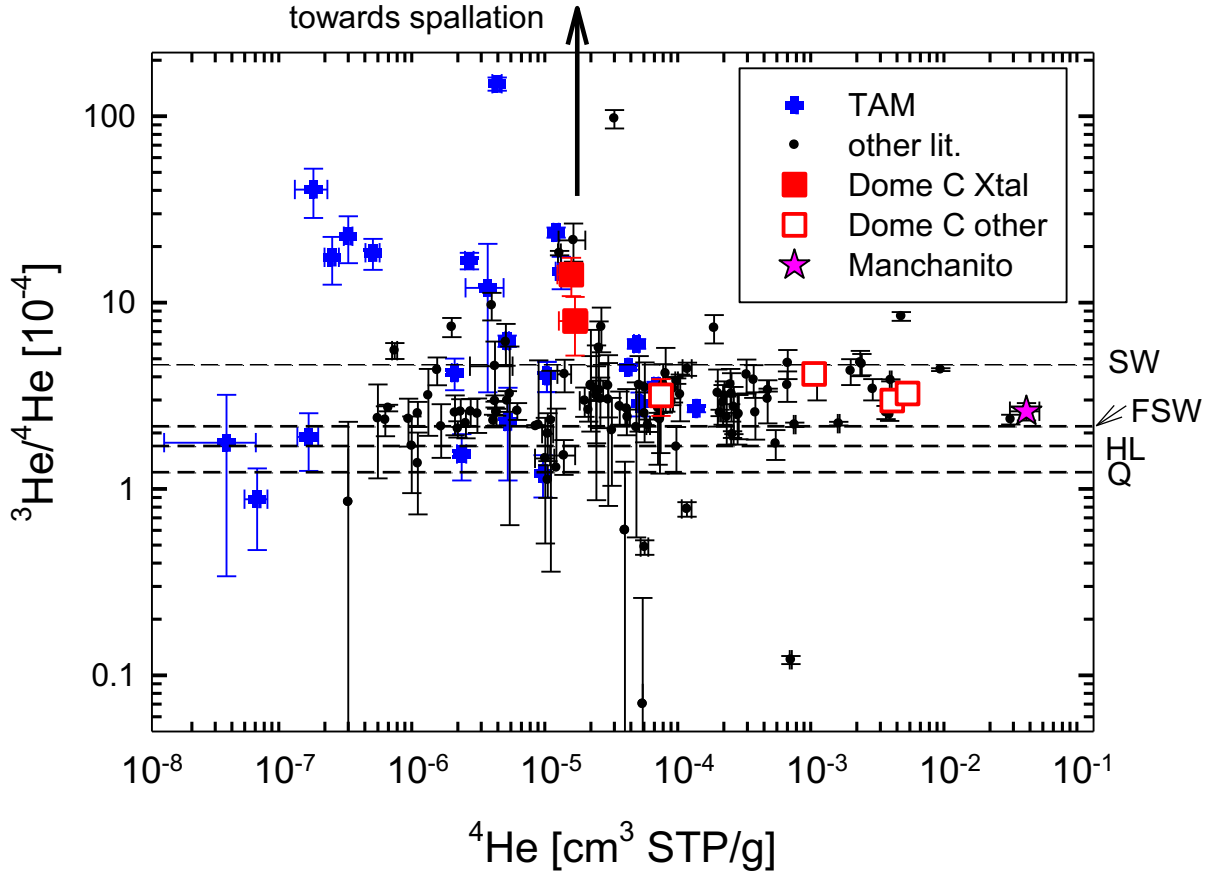

Figure 1. The ratio ^{3}He/^{4}He in 10^{-4} units is plotted vs. ^{4}He concentration in cm^3 STP/g for Dome C micrometeorites. Error bars are 1σ. Data from our previous work on TAM MMs (Baecker et al., 2018; Cordier et al., 2018) are shown for comparison, as well as data for other MMs from the literature ("other lit."): Cap Prudhomme MMs extracted from ice, from Stuart et al. (1999) and Marty et al. (2005); MMs extracted from snow at Dome Fuji (Osawa et al., 2000; Osawa and Nagao, 2002a; Okazaki et al., 2015); MMs extracted from ice near the Yamato Mountains (Osawa and Nagao, 2002b; Osawa et al. 2003b); a large MM from Greenland (Sarda et al., 1991); and the partially melted "cosmic spherule M240410 from Osawa et al. (2010). Otherwise, data for cosmic spherules are not included. Note also that this plot is somewhat biased since MMs with either ^{3}He or ^{4}He below detection limit are not included. For reference the ^{3}He/^{4}He ratios of SW (Heber et al., 2012), "FSW" (Benkert et al., 1993; Wieler et al., 2007), Q (Busemann et al., 2000) and the HL component observed in meteoritic nanodiamond residues (Huss and Lewis, 1994) are shown. Spallation He is characterized by much higher ^{3}He/^{4}He (~0.2; e.g. Wieler, 2002b) than observed here, while ^{3}He/^{4}He in the terrestrial atmosphere (1.4×10^{-6}) is lower.

Table 3. Ne and Ar results for 10 different DC MM samples from 9 different MMs as well as an additional MM from Cap Prudhomme. Uncertainties in the last digits (1σ) are given in parentheses. Where upper limits are given, these are 2σ. For comparison, the compositions of solar wind (SW), "fractionated solar wind" (FSW), Earth atmosphere (EA) and the primordial components Q (P1) and HL are listed at the bottom.

sample	particle #	^{22}Ne [10^{-12} cm^3 STP]	^{22}Ne [10^{-8} cm^3 STP/g]	^{20}Ne/^{22}Ne	^{21}Ne/^{22}Ne	^{36}Ar [10^{-12} cm^3 STP]	^{36}Ar [10^{-8} cm^3 STP/g]	^{40}Ar [10^{-6} cm^3 STP/g]	^{38}Ar/^{36}Ar	^{40}Ar/^{36}Ar
DC 06_07_213	PL 09_20 3 (1)	0.83 (3)	77.58 (7.76)	11.17 (29)	0.028 (2)	2.79 (34)	261 (32)	528 (65)	0.1841 (33)	202 (5)
DC 06_08_01	PL06_09A 1	3.22 (5)	234.9 (17.6)	11.43 (12)	0.032 (1)	2.61 (32)	190 (23)	37 (21)	0.2051 (38)	19.7 (10.8)
DC 06_09_11	PL 07_01A 11	0.52 (3)	40.62 (3.82)	11.71 (45)	0.033 (2)	2.14 (27)	165 (21)	178 (27)	0.1906 (41)	107 (9)
DC 06_09_50	PL 07_02B 2	3.89 (6)	117.8 (4.0)	12.27 (11)	0.032 (1)	19.7 (2.1)	596 (65)	181 (25)	0.1935 (23)	30.4 (2.6)
DC 06_09_57	PL07_02B 9 (1)	< 0.07	< 46.91	--	--	0.299 (132)	199 (88)	473 (22)	0.1726 (189)	237 (34)
DC 06_09_57	PL07_02B 9 (2)	< 0.07	< 771	--	--	2.98 (14)	37238 (1792)	76020 (4009)	0.1495 (39)	204 (4)
DC 06_09_63	PL07_02C 3	1.76 (10)	53.22 (3.56)	11.88 (41)	0.031 (2)	10.8 (4)	327 (14)	557 (30)	0.1830 (20)	170 (6)
DC 06_09_141	PL07_04C 9 (1)	0.22(2)	31.66 (5.69)	11.14 (85)	0.025 (4)	0.512 (132)	73.2 (18.8)	104 (31)	0.1731 (116)	142 (23)
DC 06_09_149	PL07_05A 5 (1)	2.06 (4)	688.0 (229.7)	11.65 (14)	0.032 (1)	8.64 (21)	2881 (70)	162 (108)	0.1863 (36)	5.62 (3.76)
DC 06_09_189	PL07_06A 9	3.09 (5)	309.1 (31.4)	11.89 (11)	0.032 (1)	14.6 (3)	1458 (31)	3177 (74)	0.1848 (36))	218 (2)
CP 9-1-1994	PL 10-109-D9	0.18 (3)	2.89 (52)	11.94 (97)	0.028 (5)	1.16 (5)	18.7 (8)	9.77 (72)	0.1719 (177)	52.1 (3.2)

component	references	^{20}Ne/^{22}Ne	^{21}Ne/^{22}Ne	^{38}Ar/^{36}Ar	^{40}Ar/^{36}Ar
SW	[1]	13.777 (10)	0.03289 (7)	0.183 (1)	
"FSW"	[2, 3]	11.2 (2)	0.0295 (5)	0.205 (2)	
Q (P1)	[4]	10.67 (2)	0.0294 (10)	0.187 (1)	
EA	[5, 6]	9.80	0.029	0.1885 (3)	298.56 (31)
HL	[7]	8.50 (6)	0.036 (1)	0.227 (3)	

References: [1] Heber et al. (2012); [2] Benkert et al. (1993); [3] Wieler (2002a); [4] Busemann et al. (2000), the ^{20}Ne/^{22}Ne ratio is the mean for Q-Ne from Allende, Murchison, Grosnaja and Chainpur; [5] Eberhardt et al. (1965); [6] Lee et al. (2006); [7] Huss and Lewis (1994); Note: For more information regarding **"**FSW**"** see Wieler et al. (2007).

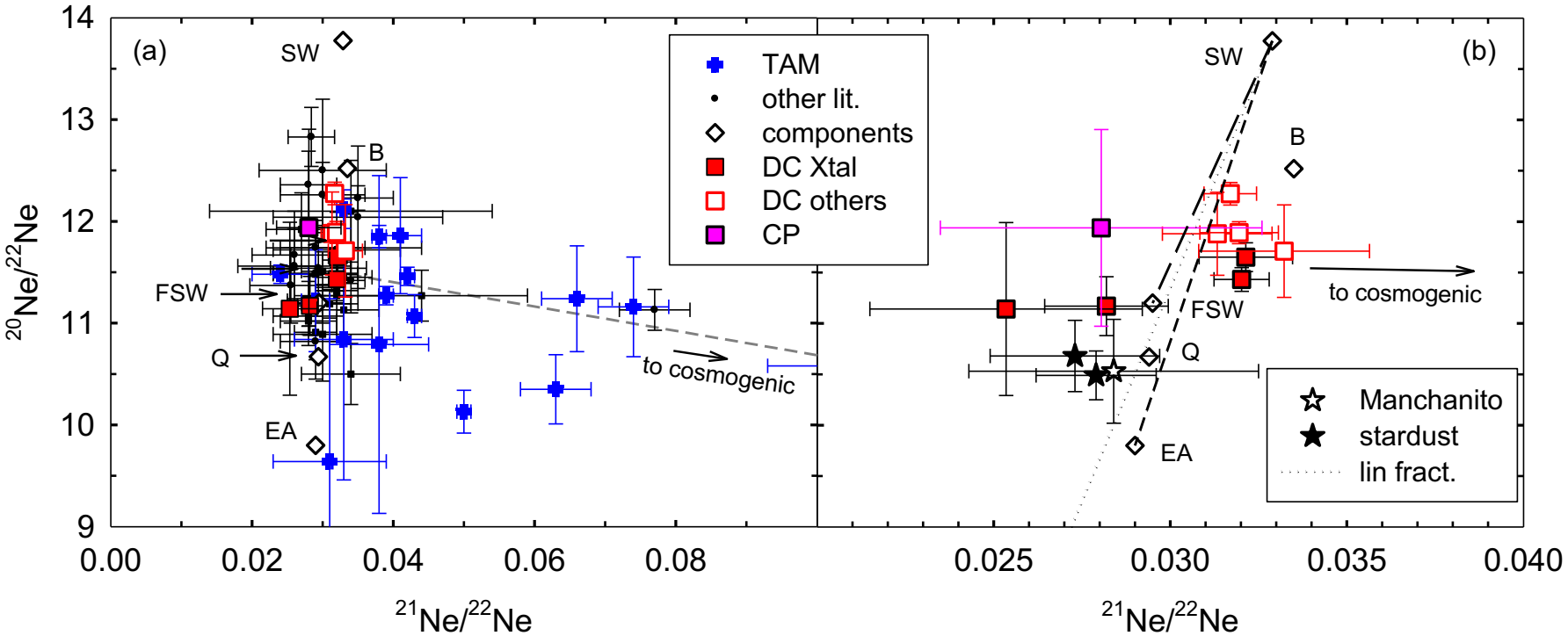

346

347 Figure 2: Three isotope plots of $^{20}Ne/^{22}Ne$ vs. $^{21}Ne/^{22}Ne$. Crystalline (Xtal) and other DC MMs are distinguished by different symbols. Error bars are 1 σ.
348 Plotted for reference are the trapped compositions SW (Heber et al., 2012), Ne-B (Black and Pepin, 1969), "FSW" (Benkert et al., 1993 and Wieler et al.,
349 2007), Q (P1) (Busemann et al., 2000), Earth atmosphere (EA) (Eberhardt et al., 1965), and HL (Huss and Lewis, 1994).
350 a) For comparison, MM data from Dome Fuji (Osawa et al., 2000; Osawa and Nagao 2002a; Okazaki et al. 2015) and from the Yamato ice field (Osawa
351 and Nagao, 2002b; Osawa et al., 2003b) are included, as well as such from our earlier report on MMs from the Transantarctic Mountains (TAM: separate
352 symbols; Baecker et al., 2018). In order not to clutter the diagram, only literature data with an error of less than 0.5 in the $^{20}Ne/^{22}Ne$ ratio are shown. Some
353 scoriaceous TAM MMs fall outside the plotted range, shifted towards a cosmogenic composition.
354 b) More detailed view of the DC MMs. Mixing lines SW-FSW and SW-EA, and the mass fractionation line (linear law) originating at the solar wind
355 composition (Heber et al., 2012) are shown for reference, furthermore the composition measured for the IDP Manchanito (Ogliore et al., 2020) and the
356 two more precise analyses of stardust track 41, aerogel cell C2044 (St-1 and Thera-2; Marty et al., 2008).

Fig. 2b shows the range between $^{21}Ne/^{22}Ne$ = 0.02 and 0.04 in more detail and concentrates on the samples of this study. Interestingly, as for He, there is a distinction between the MMs classified as Xtal and the others. The latter (i.e., the non-Xtal), together with two of the Xtal MMs, show higher $^{20}Ne/^{22}Ne$ than the other two crystalline MMs. Compared to mixing lines between SW and FSW or EA, and also compared to compositions for (linearly) mass fractionated SW, these MMs show a small shift towards elevated $^{21}Ne/^{22}Ne$, indicative of small cosmogenic contributions. On the other hand, Xtal DC 06_07_213 and Xtal 06_09_141 (as well as, with large error, the CP MM) plot to the left of these lines. Their position is similar, although at somewhat higher $^{20}Ne/^{22}Ne$, to what has been observed for the IDP Manchanito (Ogliore et al., 2020) and in the two more precise analyses of cometary Ne in stardust track 41, aerogel cell C2044 (Marty et al., 2008). The significance of these observations will be discussed in chapter 4.5.

3.2. Argon

Results for Ar are given in Table 3 and depicted in a three-isotope plot of $^{40}Ar/^{36}Ar$ vs. $^{38}Ar/^{36}Ar$ (Fig. 3). Except for the special case of DC 06_09_ (see below), all of our MMs contain substantial concentrations of ^{36}Ar (~7 x 10^{-7} to ~3 x 10^{-5} cm^3 STP/g), along with $^{40}Ar/^{36}Ar$ below the air ratio, thus clearly of extraterrestrial origin. Ratios of $^{40}Ar/^{36}Ar$ range from ~6 (Xtal DC 06_09_149) up to ~218 (Fg/Sc DC 06_189). The former is also characterized by the highest concentration of (extraterrestrial) ^{36}Ar, while the higher ratio for the latter may not be surprising, since it is partly scoriaceous, and because scoriaceous MMs are more likely to be contaminated by air Ar (Baecker et al., 2018).

Ratios of $^{20}Ne/^{36}Ar$ are in the range 2 to 5, with the exception of DC 06_08_01 (~14). This is much lower than in the solar wind (~42; Heber et al., 2012; Vogel et al., 2009) and only the latter value is similar to what we have previously estimated for FSW (~12; Baecker et al., 2018; based on data from Benkert et al., 1993). It appears likely, therefore that for Ar, besides the solar wind contribution, there are also contributions from air and/or from primordial trapped components such as Q. However, the implied extent depends very much on how strongly fractionated the Ne/Ar ratio of the solar component is. This conclusion is borne out by the position of the data points in Fig. 3, where several (with small errors) in $^{38}Ar/^{36}Ar$ plot close to the composition of SW, perhaps slightly shifted towards air/Q. A few are further enhanced in this ratio, in particular DC 06_08_01. Presence of cosmogenic ^{38}Ar would offer an explanation, in principle, but this appears unlikely by comparison with the concentration of cosmogenic ^{21}Ne (chapter 3.4). Notably, $^{38}Ar/^{36}Ar$ for this MM happens to agree with that of pure FSW.

There are four cases where $^{38}Ar/^{36}Ar$ is lower than in SW, which has the lowest value among the reference compositions that are shown. Three of them have very large uncertainties and within 1σ overlap with SW, so we do not take this as significant. The fourth case is the second specimen from DC 06_09_57 (labeled in Fig. 3), which we omitted in the discussion above. This sample has by far the highest nominal concentration of ^{36}Ar of ~3.7 x 10^{-4} cm^3 STP/g – note that this has been the smallest analyzed sample by far and that uncertainties in sample weight are not included in the errors given in Table 3. As it happens, the combination of $^{38}Ar/^{36}Ar$ and $^{40}Ar/^{36}Ar$ could also result from mass-fractionated air Ar (with, possibly, a small addition of radiogenic ^{40}Ar), but the mass fractionation would have to be enormous and

would have to favor the light isotopes, a very unusual situation. While one may also think of overcorrection for blank or isobaric interferences as a reason, this is also unlikely since the actual amount (rather than concentration) is not especially low in this sample. This is thus a surprising result, and we note that the same sample appears also to be unique in Xe, and that these two results might be related (chapter 4.5).

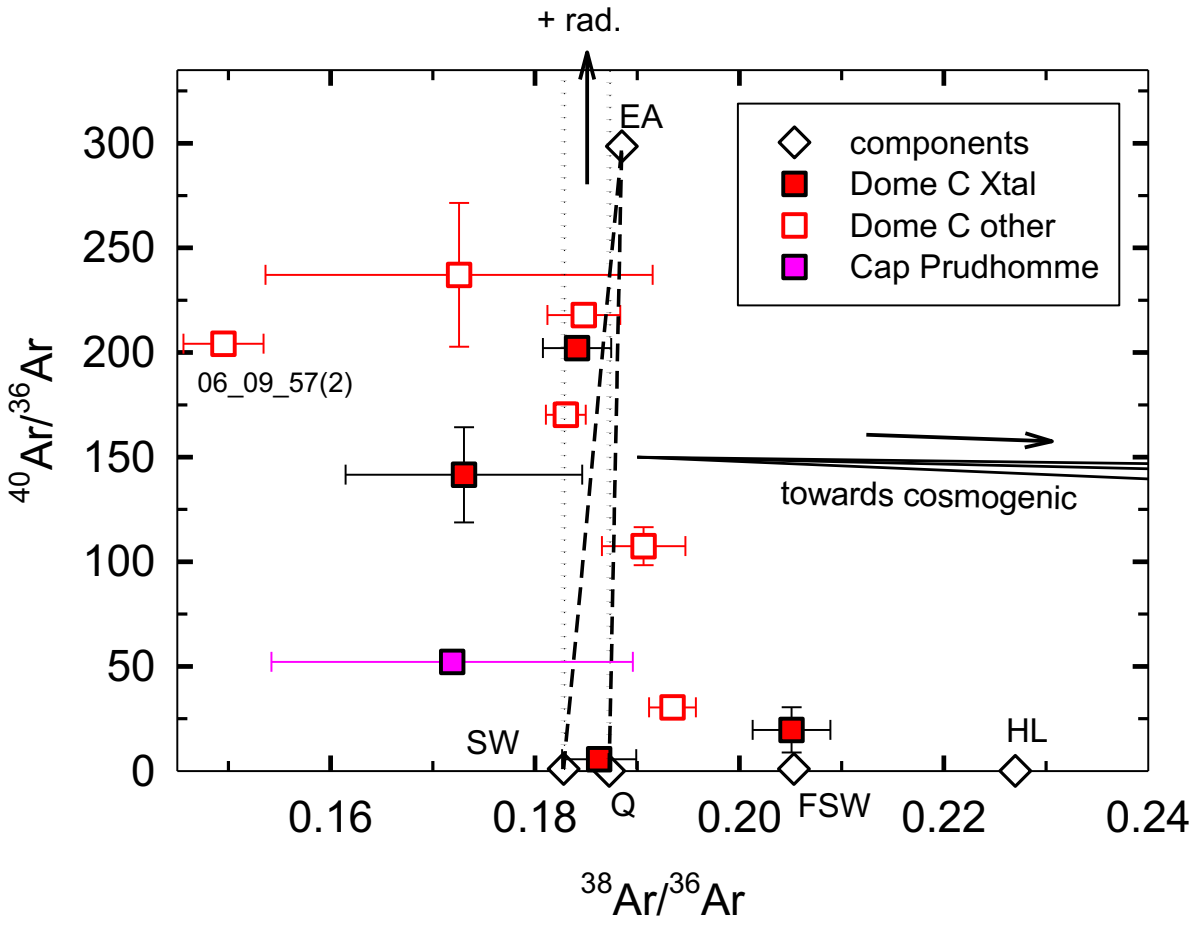

Figure 3: Three-isotope plot of $^{40}Ar/^{36}Ar$ vs. $^{38}Ar/^{36}Ar$ for, with 1σ error bars, separately for crystalline (Xtal) and "other" MMs. Plotted for reference are the compositions of SW (Heber et al., 2012), "FSW" (Wieler, 2002a and Wieler et al., 2007), Q (P1) (Busemann et al., 2000), Earth atmosphere (EA) (Lee et al., 2006), and HL (Huss and Lewis, 1994). The dotted lines indicate the position of data points with SW-like and Q-like $^{38}Ar/^{36}Ar$ and variable $^{40}Ar/^{36}Ar$ due to addition of radiogenic ^{40}Ar, in order to guide the eye, while the dashed lines show the effects of mixing either SW-Ar or Q-Ar with air. The solid lines trending to the right indicate the effect of mixing an "arbitrary" (roughly in the center of the plot) composition with three types of cosmogenic Ar, which, on the scale of the plot, are almost indistinguishable. From top to bottom these are: cosmogenic Ar produced by GCR in MMs (Trappitsch and Leya, 2013); cosmogenic Ar as typically found in meteorites (Wieler et al., 2002b); cosmogenic Ar produced in MMs by solar cosmic rays characterized by a rigidity of 100 MV (Trappitsch and Leya, 2013). CM chondrite chemical composition was assumed for the production in MMs. Ar in the coma of comet 67/P Churyumov-Gerasimenko has a highly uncertain $^{38}Ar/^{36}Ar$ ratio of 0.185±0.048 (Rubin et al., 2018), and a $^{40}Ar/^{36}Ar$ ratio has not been reported.

3.3. Krypton and Xenon

Tables 4 and 5 summarize the Kr and Xe results. Not listed are the rare isotopes ^{78}Kr, ^{124}Xe and ^{126}Xe, for which no useful isotopic data were obtained. It is clear, though, that the abundances of these isotopes are low. As a consequence, there are no significant cosmogenic contributions that would make a noticeable effect on the ratios of the heavier, more abundant, isotopes. Kr and Xe were not detectable or indistinguishable from blank in two MMs: Xtal DC 06_09_141 and the first (larger) of the DC 06_09_57 samples. Note that Spring (2014) also did not find detectable Xe in their analysis of another portion of DC 06_09_57. Additionally, krypton was not detectable in the scoriaceous Cap Prudhomme MM CP 9-1-1994.

Like in Ar, the second DC 06_09_57 sample is characterized by extremely high nominal concentrations of Kr and Xe. While this is the smallest analyzed sample by far - with associated large uncertainty in weight, which is not included in the nominal errors given in the tables - this hardly offers an explanation for the much higher nominal concentrations, by roughly two orders of magnitude in case of Kr (not counting DC 06-09_189, which is only ~3x lower). Otherwise, Kr concentrations range between ~1 and ~3 x 10^{-8} cm^3 STP/g (~1 to~7 x 10^{-14} cm^3 STP). Measured amounts of ^{132}Xe range from ~1 x 10^{-15} cm^3 STP to ~2 x 10^{-13} cm^3 STP, with concentrations mostly below 10^{-8} cm^3 STP/g. The most notable exception, besides DC_06_189, is, again, the second fragment of DC 06_09_57. This is, while the first fragment of this MM, like the one analyzed by Spring (2014), was below detection limit.

Concerning isotopes of Kr, data scatter mostly around common trapped components (EA, Q, SW), but SW is unlikely to make significant contributions to either Kr or Xe in most cases, given the concentrations of the lighter elements and the relative abundances in the solar wind (see chapter 4.3). Uncertainties in measured isotopic compositions are large compared to diagnostic differences, anyway. The only possible exception is Xtal DC 06_07_213, which may show a slight mass fractionation effect. While otherwise this sample does not stand out, its position is similar in the three-isotope plots for Xe presented in Fig. 4, where the dotted and dashed lines show the effect of mass fractionation starting with the composition of Q-Xe and EA, respectively.

Isotopic ratios plotted in Fig. 4 are ^{136}Xe/^{132}Xe on the ordinate vs. ^{134}Xe/^{132}Xe (Fig. 4a) and ^{130}Xe/^{132}Xe (Fig. 4b) on the abscissa. Xtal DC06_09_149 had the smallest measured amount of Xe and its isotopic data have extremely large uncertainties. The nominal values plot off scale. Reference compositions that are shown are SW, Q, EA (see Figure Caption for references). Two mixing lines are shown in each figure: one (solid black line trending upwards) between Q and HL-Xe, the Xe carried by presolar nanodiamond, and another between Q-Xe and Xe with the composition of cometary Xe (dashed dark cyan line), as inferred from measurements in the coma of comet 67P/Churyumov-Gerasimenko by Marty et al. (2017). The latter trends downwards.

Table 4. Kr results for DC micrometeorites ("DC") and a single MM from Cap Prudhomme ("CP"). No data are reported for the rare ^{78}Kr isotope. Uncertainties in the last digits (1σ) are given in parentheses, where the uncertainty in sample weight is not included in the error of the concentration. For comparison, the compositions of solar wind (SW), Earth atmosphere (EA) and the primordial components Q(P1) and HL are listed at the bottom.

sample	**particle #**	**^{84}Kr [10^{-14} cm^3 STP]**	**^{84}Kr [10^{-8} cm^3 STP/g]**	**^{80}Kr/^{84}Kr**	**^{82}Kr/^{84}Kr**	**^{83}Kr/^{84}Kr**	**^{86}Kr/^{84}Kr**
DC 06_07_213	PL 09_20 7 (3)	2.71 (60)	2.54 (56)	0.035 (5)	0.198 (17)	0.201 (12)	0.331 (20)
DC 06_08_01	PL06_09A 1	1.58 (60)	1.15 (43)	0.043 (8)	0.226 (27)	0.186 (18)	0.310 (27)
DC 06_09_11	PL 07_01A 11	1.18 (59)	0.91 (46)	0.038 (11)	0.274 (36)	0.209 (26)	0.312 (37)
DC 06_09_50	PL 07_02B 2	3.87 (61)	1.17 (19)	0.038 (4)	0.209 (12)	0.200 (9)	0.288 (13)
DC 06_09_57	PL07_02B 9 (1)	< 1.22	< 8.13	--	--	--	--
DC 06_09_57	PL07_02B 9 (2)	2.06 (52)	258 (65)	0.053 (7)	0.214 (23)	0.201 (18)	0.324 (30)
DC 06_09_63	PL07_02C 3	6.86 (77)	2.08 (23)	0.045 (3)	0.215 (8)	0.206 (7)	0.287 (10)
DC 06_09_141	PL07_04C 9 (1)	< 1.04	< 1.49	--	--	--	--
DC 06_09_149	PL07_05A 5 (1)	0.94 (51)	3.13 (1.71)	0.062 (13)	0.250 (38)	0.219 (27)	0.333 (44)
DC 06_09_189	PL07_06A 9	71.58 (3.19)	3.19 (38)	0.038 (1)	0.195 (7)	0.196 (6)	0.293 (8)
CP 9-1-1994	PL 10-109-D9	< 0.50	< 0.08	--	--	--	--

component	**references**	**^{80}Kr/^{84}Kr**	**^{82}Kr/^{84}Kr**	**^{83}Kr/^{84}Kr**	**^{86}Kr/^{84}Kr**
SW	[1]	0.0412 (2)	0.2054 (2)	0.2034 (2)	0.3012 (4)
Q (P1)	[2]	0.03937 (7)	0.2018 (2)	0.2018 (2)	0.3095 (5)
EA	[3]	0.039599 (20)	0.20217 (4)	0.2014 (2)	0.3052 (3)
HL	[4]	0.0305 (10)	≡ 0.1590	0.1989 (10)	0.3623 (18)

References: [1] Meshik et al. (2014); [2] Busemann et al. (2000); [3] Basford et al. (1973); [4] Huss and Lewis (1994) as re-calculated by Busemann et al. (2000).

Table 5. Xe results for DC micrometeorites ("DC") and a single MM from Cap Prudhomme ("CP"). No data are reported for the rare isotopes ^{124}Xe and ^{126}Xe. Uncertainties in the last digits (1σ) are given in parentheses, where the uncertainty in sample weight is not included in the error of the concentration. For comparison, the compositions of solar wind (SW), Earth atmosphere (EA) and the primordial components Q(P1) and HL are listed at the bottom.

sample	particle #	^{132}Xe [10^{-14} cm^3]	^{132}Xe [10^{-8} cm^3 STP/g]	^{128}Xe/^{132}Xe	^{129}Xe/^{132}Xe	^{130}Xe/^{132}Xe	^{131}Xe/^{132}Xe	^{134}Xe/^{132}Xe	^{136}Xe/^{132}Xe
DC 06_07_213	PL 09_20 7 (3)	0.91 (19)	0.85 (18)	0.060 (11)	0.947 (47)	0.135 (8)	0.841 (46)	0.412 (24)	0.394 (30)
DC 06_08_01	PL06_09A 1	0.39 (18)	0.28 (13)	0.041 (23)	0.921 (78)	0.137 (16)	0.632 (75)	0.431 (48)	0.342 (49)
DC 06_09_11	PL 07_01A 11	1.01 (19)	0.78 (15)	0.083 (10)	1.033 (44)	0.166 (9)	0.783 (40)	0.370 (21)	0.333 (24)
DC 06_09_50	PL 07_02B 2	2.87 (25)	0.87 (7)	0.072 (5)	0.995 (23)	0.162 (4)	0.784 (19)	0.397 (11)	0.349 (13)
DC 06_09_57	PL07_02B 9 (1)	< 0.17	< 1.12	--	--	--	--	--	--
DC 06_09_57	PL07_02B 9 (2)	0.20 (8)	24.53 (10.21)	0.102 (64)	1.200 (139)	0.135 (48)	0.746 (157)	0.312 (78)	0.159 (91)
DC 06_09_63	PL07_02C 3	1.79 (26)	0.54 (8)	0.084 (8)	0.980 (31)	0.167 (6)	0.777 (29)	0.368 (16)	0.334 (18)
DC 06_09_141	PL07_04C 9 (1)	< 0.14	< 0.20	--	--	--	--	--	--
DC 06_09_149	PL07_05A 5 (1)	0.11 (8)	3.53 (27)	0.028 (112)	0.911 (210)	0.124 (86)	0.898 (254)	0.384 (134)	0.513 (182)
DC 06_09_189	PL07_06A 9	17.27 (26)	17.27 (26)	0.073 (2)	0.991 (14)	0.153 (2)	0.782 (9)	0.386 (5)	0.318 (5)
CP 9-1-1994	PL 10-109-D9	0.90 (6)	0.14 (1)	0.077 (10)	1.035 (46)	0.158 (9)	0.869 (41)	0.362 (24)	0.299 (29)

component	references	^{128}Xe/^{132}Xe	^{129}Xe/^{132}Xe	^{130}Xe/^{132}Xe	^{131}Xe/^{132}Xe	^{134}Xe/^{132}Xe	^{136}Xe/^{132}Xe
SW	[1]	0.0842 (2)	1.0405 (10)	0.1648 (3)	0.8256 (12)	0.3698 (6)	0.3003 (5)
Q (P1)	[2]	0.0822 (2)	1.042 (2)	0.1619 (3)	0.8185 (9)	0.3780 (11)	0.3164 (8)
EA	[3]	0.07136 (9)	0.9832 (12)	0.15136 (12)	0.7890 (11)	0.3879 (6)	0.3294 (4)
HL	[4]	0.0905 (6)	1.056 (2)	0.1542 (3)	0.8457 (13)	0.6356 (13)	≡ 0.6991

References: [1] Meshik et al. (2015); [2] Busemann et al. (2000); [3] Basford et al. (1973); [4] Huss and Lewis (1994) as re-calculated by Busemann et al. (2000)).

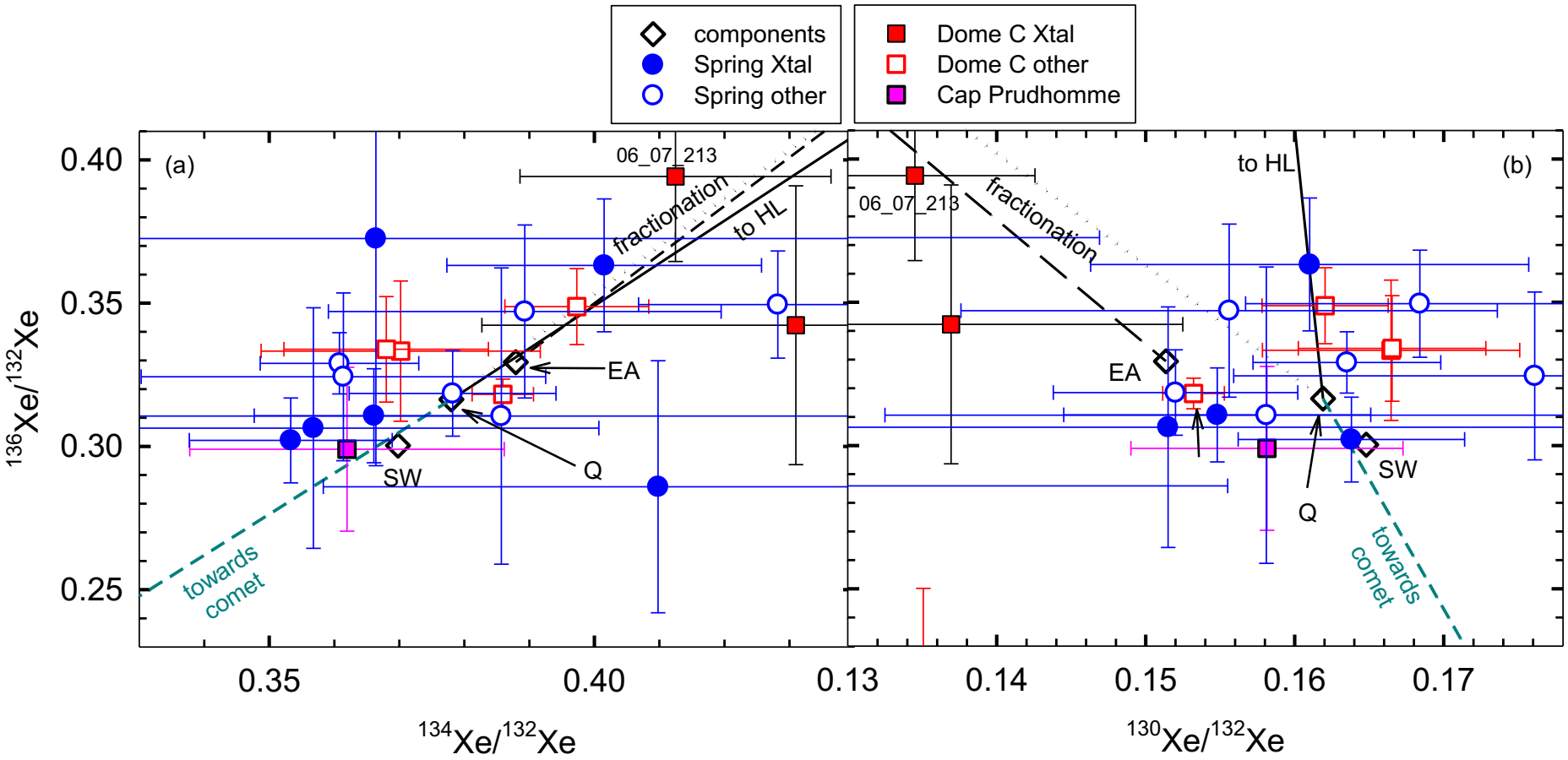

Figure 4. Three-isotope plots of $^{136}Xe/^{132}Xe$ vs. $^{134}Xe/^{132}Xe$ (a) and vs. $^{130}Xe/^{132}Xe$ (b). Data points for crystalline and other MM samples are shown separately. Error bars are 1 σ. DC 06_09_149 with very large uncertainties is not shown, while DC 06_09_57 (2) is off scale and discussed separately (chapter 4.5). Plotted for comparison are the compositions of air (Basford et al., 1973), Q-Xe (Busemann et al., 2000) and Xe-HL (Huss and Lewis, 1994; as recalculated by Busemann et al., 2000). Data from Spring (2014) obtained for MMs from Dome C and Cap Prudhomme are also included. The dotted and the dashed lines show the trend expected for mass fractionation starting from Q and air composition, respectively, while the solid line is the mixing line between Q and HL-Xe The dashed dark cyan lines are mixing lines between Q-Xe and Xe as reported for the coma of comet 67P/Churyumov-Gerasimenko by Marty et al. (2017).

Besides our own results, we have included in Fig. 4 data from Spring (2014), who obtained data for Xe in the same MMs from Dome C analyzed here. Like our data, the Spring data are distinguished in Fig. 4 between MMs classified as Xtal and others. Good agreement is observed between her and the two data sets, but the uncertainties are large in both cases, due to the small gas amounts analyzed. The Spring (2014) data do not include DC 06_09_57, since Xe was not above extraction blank level. Again, this is in agreement with our result for the larger fragment we analyzed from this MM. The smaller fragment that we analyzed, however, turned out different, having strange Ar isotopes (chapter 3.2), with very high abundances of Ar and Kr, and comparably high Xe abundance. Concerning isotopes of Xe, this fragment is also unique, with very low $^{134}Xe/^{132}Xe$ and $^{136}Xe/^{132}Xe$. It plots off scale in Fig. 4, and we will return to this observation below (chapter 4.5).

3.4. Cosmogenic noble gases

Contributions from cosmogenic noble gases in meteorites are commonly observed as excesses of ^{21}Ne, ^{3}He and, less frequently, ^{38}Ar. Such excesses are clearly visible only in few of our MMs. This contrasts with the situation in the TAM MMs of Baecker et al. (2018), but is similar to the majority of MMs analyzed in other previous studies (Dome Fuji and Yamato: Osawa et al., 2000, 2003; Osawa and Nagao, 2002a, 2002b; Okazaki et al., 2015), the reason being the high abundances of solar wind noble gases. For Ne, this is obvious in Fig. 2, where Fig. 2a shows a comparison with the previous data, and Fig. 2b shows in more detail that our data points plot close to trapped compositions that one might expect to be present: mixtures of solar wind proper (SW; Heber et al., 2012) with fractionated solar wind (FSW; Benkert et al., 1993), Q (Ott, 2014) and Earth atmosphere, or simply mass fractionated solar wind (the dotted line).

Obviously, the data points to the left of the lines in Fig. 2b show no evidence of cosmogenic Ne. Six others plot to the right, and we list in Table 6 the inferred concentrations of cosmogenic ^{21}Ne, together with the concentrations of trapped ^{20}Ne. We list two sets of values obtained by using two different reference trapped compositions. However, as also obvious in Fig. 2b, differences between the two approaches are small compared to the analytical errors. In one approach, following Baecker et al. (2018) to whom we refer for more detail, the numbers were obtained from a 3-component deconvolution: a cosmogenic endmember (with negligible influence of the exact choice), and two "trapped" endmembers, namely "fractionated solar wind" Ne (FSW; Benkert et al., 1993) and solar-wind Ne (SW; Heber et al., 2012), as given in Table 3. The other approach, which was also used by, e.g., Schmitz et al. (2019) in their study of fossil MMs, was simply considering the excess ^{21}Ne over the composition of (linearly) mass fractionated solar wind. Uncertainties of the reference compositions were taken into account in calculating the listed uncertainties. Two additional entries in Table 6 are upper limits for the two samples from DC 06_09_57, corresponding to the actually measured amounts of ^{21}Ne.

Table 6. Concentrations of cosmogenic ^{3}He, ^{21}Ne as well as "cosmogenic" ^{38}Ar and concentration of trapped ^{20}Ne. Units are 10^{-8} cm^3 STP/g, errors (1σ) are in parentheses. The cosmogenic abundances are sensitive to assumptions about the composition of the trapped components, and two different sets have been used for both Ne and He, as described in the text. In case of cosmogenic ^{21}Ne, the upper values are those obtained from 3-component resolution, while the lower values correspond to excesses over the linearly fitted SW mass fractionation line. For cosmogenic ^{3}He, the upper values are those obtained from an assumed SW/FSW mixing ratio for the trapped component derived from the Ne data, while the lower values assume a constant $3x10^{-4}$ for trapped $^{3}He/^{4}He$. In case of DC 06:09_57 the listed upper limits (2σ) correspond to total measured abundances instead. The case for the nominally high abundance of cosmogenic ^{3}He in DC 06_09_189 is marginal and listed in italics and small print. Evidence for "cosmogenic" ^{38}Ar (calculated for the two cases with high $^{38}Ar/^{36}Ar$ in Fig. 3, following Baecker et al., 2018) is also marginal and the values are listed in italics and small print as well.

sample	particle #	$^{21}Ne_{cos}$	$^{20}Ne_{tr}$	$^{3}He_{cos}$	$^{38}Ar_{cos}$
DC 06_07_213	PL 09_20 3 (1)	--	867 (90)	0.90 (24) 0.77 (24)	--
DC 06_08_01	PL06_09A 1	0.53 (18) 0.41 (15)	2684 (51)	1.67 (24) 1.54 (24)	< 4.4
DC 06_09_11	PL 07_01A 11	0.13 (7) 0.11 (7)	475 (31)	0.30 (51) 0.12 (47)	--
DC 06_09_50	PL 07_02B 2	0.09 (4) 0.06 (3)	1445 (25)	< 4.28 < 16.66	*2.5 (2.2)*
DC 06_09_57	PL07_02B 9 (1)	< 1.00	< 251	< 3.62	--
DC 06_09_57	PL07_02B 9 (2)	< 12.66	< 5146	--	--
DC 06_09_63	PL07_02C 3	0.05 (4) 0.03 (4)	632 (43)	12.48 (4.35) 10.92 (2.92)	--
DC 06_09_141	PL07_04C 9 (1)	--	353 (47)	--	--
DC 06_09_149	PL07_05A 5 (1)	1.44 (67) 1.13 (62)	8014 (188)	--	--
DC 06_09_189	PL07_06A 9	0.49 (21) 0.36 (18)	3675 (73)	*19.23 (6.75)* *12.30 (10.40)*	--
CP 9-1-1994	PL 10-109-D9	--	35 (7)	< 0.45	--

For cosmogenic ^{3}He, except for two Xtal MMs (DC 06_07_213 and DC 06_08_01) which clearly plot at higher $^{3}He/^{4}He$ than all trapped compositions (Fig. 1), results (or, for that matter, the mere evidence for presence of cosmogenic ^{3}He) depend sensitively on the choice for the trapped ratio. Again, we list the results for two cases: in one case, again following Baecker et al. (2018), we chose a composition for trapped $^{3}He/^{4}He$ assuming the same mixing ratio (and nominal uncertainties) between SW and FSW for He as inferred for Ne. Since in some cases, notably DC 06_09_63 and DC 06_09_189, the so obtained results appeared unrealistic, and, since, in Fig. 1, $^{3}He/^{4}He$ for high (>10^{-4} cm^3 STP/g) ^{4}He concentrations seems to level off at ~3 x 10^{-4}, we used this value for the trapped component in the alternative approach. An error of 0.2 x 10^{-4} in this ratio was propagated in this case. For the cosmogenic component, we used $^{3}He/^{4}He = 0.20 \pm 0.05$ in both cases, but, as in Ne, the exact choice of the cosmogenic composition has essentially no influence in the calculation of its abundance. With

the alternative assumption for the composition of the trapped component, the nominally high cosmogenic ^{3}He abundance in DC 06_09_189 becomes a marginal case, but the abundance in DC 06_09_63 remains high. We note that the measured ratio in this MM is still below the ratio for unfractionated SW and so, in principle, the possibility remains that this cosmogenic ^{3}He is not real. By comparison with other MMs it appears unlikely, however, to have such a high trapped ^{3}He/^{4}He ratio (see also chapter 4.4).

As for ^{38}Ar, there are two MMs that clearly show enhanced ^{38}Ar/^{36}Ar relative to SW, "planetary" (Q) and air: DC 06_08_01 (Xtal) and DC 06_09_50 (FgC). The high ratios may, in principle, be explained by addition of cosmogenic Ar. We have therefore calculated nominal abundances of cosmogenic ^{38}Ar using the approach of Baecker et al. (2018), where contributions to trapped Ar from SW, FSW and planetary Ar are estimated from the SW/FSW mixing ratio at Ne and the Ne/Ar ratio of the different components. The values are listed in Table 6, but obviously, cosmogenic contributions are difficult to ascertain even in these two cases. We will not consider cosmogenic ^{38}Ar in chapter 4.4.

4. Discussion

4.1. Noble gas general pattern

We will concentrate on the MMs from Dome C in this discussion. The single particle from Cap Prudhomme, although being of larger size, is scoriaceous rather than primitive and has low noble gas abundances and, therefore, does not add information.

As common in meteorites with implanted solar wind, the light noble gases He and Ne of the MMs from Dome C analyzed in this work are dominated by the trapped solar wind component, while for heavy Kr and Xe a trapped "planetary" component (Ott, 2014) accounts for most of the inventory. Argon generally represents a mixed case. Here we present a short general overview of abundances, while in the following sections (4.2 and 4.3), we will discuss the individual cases in more detail. We show an overview of the trapped noble gas abundances in Figure 5 (crystalline MMs, left; others, right). The concentrations of the major isotopes are plotted, and, since MMs have often been compared to CM meteorites (Kurat et al., 1994; Engrand and Maurette, 1998), we normalized them to the concentrations in CM meteorites, where we considered CM Maribo #2 as reported in Haack et al. (2012) as representative, as we did in Baecker et al. (2018). Again, the possible, but probably small, radiogenic contributions to ^{4}He are ignored. Shown are the individual specimens as well as the geometric means for the two populations. For comparison, we also show the geometric means for the TAM MMs of Baecker et al. (2018) and for the Antarctic MMs collected at Dome Fuji and in the Yamato Mountain area as reported by Osawa et al. (2000), Osawa and Nagao (2002a, b) and Osawa et al. (2003b). Data on another suite of Dome Fuji samples analyzed by Okazaki et al. (2015) are shown separately, while, for the geometric mean of TAM MMs, we distinguish between scoriaceous and unmelted MMs.

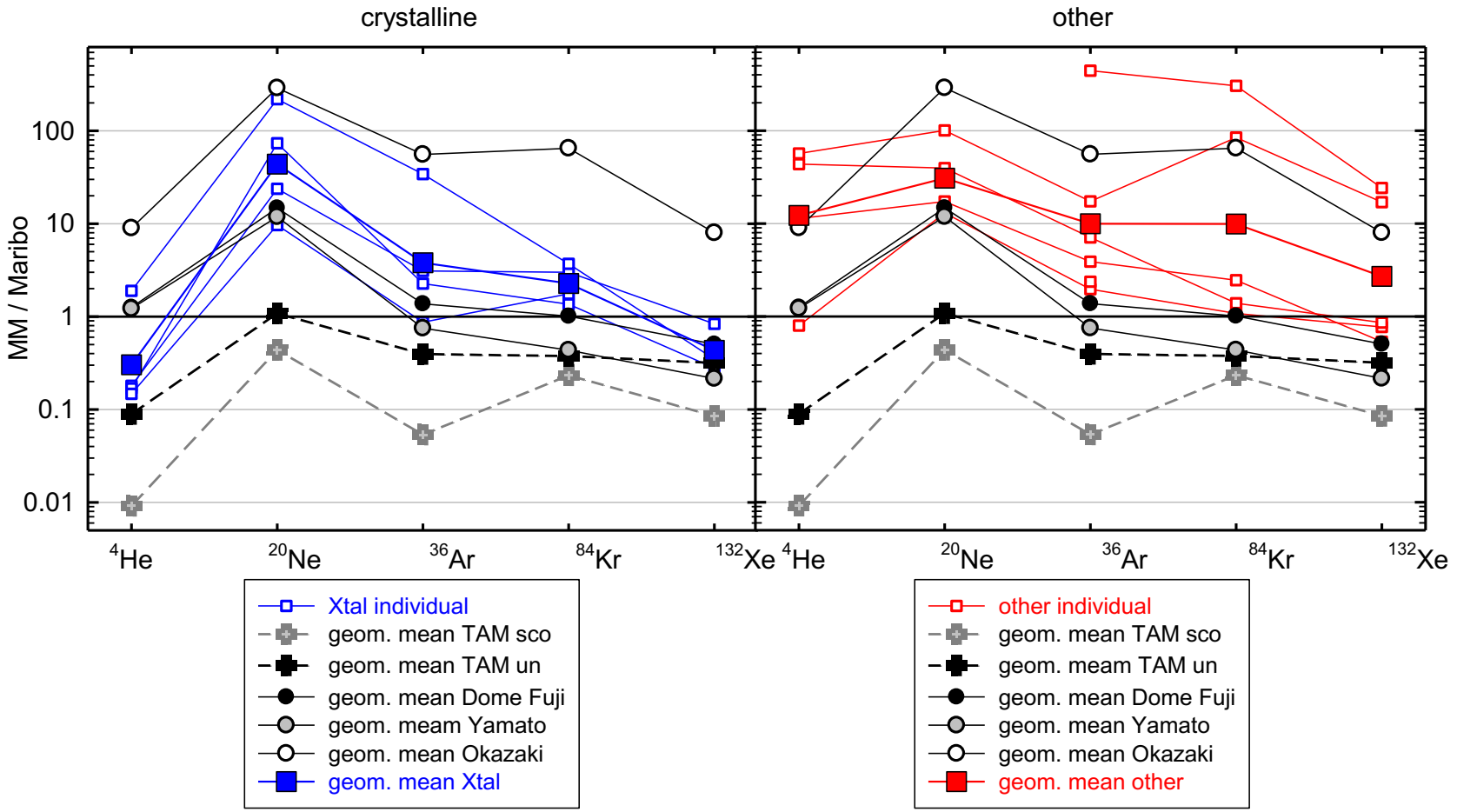

584

585 Figure 5. Noble gas concentrations in DC MMs, normalized to CM Maribo #2 (Haack et al., 2012). Shown are the individual specimens
586 as well as the geometric means for the two populations (Xtal and "other") separately. For comparison we also show the geometric means
587 for the TAM MMs of Baecker et al. (2018) and for Antarctic MMs collected at Dome Fuji and in the Yamato Mountain (Osawa et al.,
588 2000; Osawa and Nagao, 2002a, b; Osawa et al., 2003b). Data the Dome Fuji samples of Okazaki et al. (2015) are shown separately, while
589 for the geometric mean of TAM MMs we distinguish between scoriaceous and unmelted MMs.

590 Several features are apparent. First, the scoriaceous MMs show, by far, the lowest noble
591 gas concentrations. This is to be expected given the higher temperature experienced by
592 scoriaceous (partly melted) micrometeorites during atmospheric entry, resulting in more severe
593 gas loss. Nevertheless, concentrations also in the unmelted TAM MMs are lower than in the
594 other MMs, in particular for He and Ne. The larger sizes of the TAM MMs (~600 μm on
595 average; Baecker et al., 2018) compared to the Dome Fuji and Yamato Mountain MMs as well
596 as our DC MMs, and the correspondingly lower surface to volume ratio of TAM MMs may
597 have played a role, since He and Ne are predominantly of solar wind origin and thus surface-
598 correlated (implantation depth < 0.1 μm). Second, in accordance with such an interpretation,
599 on average the concentrations of (volume-correlated) Xe in the unmelted TAM MMs are not
600 too different from those of the Dome Fuji and Yamato Mountains MMs of Osawa et al. (2000,
601 2003b) and Osawa and Nagao (2002a, b), as well as the reference CM meteorite, for that matter.
602 This similarity holds also in comparison with the majority of our DC MMs, although at least
603 two of the latter show significantly higher concentrations, raising the mean for our DC samples
604 above those reference abundances.

605 Third, the average concentrations reported by Okazaki et al. (2015) for MMs recovered
606 from surface snow near Dome Fuji are one to two orders of magnitude higher than the others
607 reported previously, but are roughly matched by some of our DC MMs. The similarity between
608 the two sets of data is striking and most probably related to the collection method. Our Dome
609 C and the Dome Fuji particles of Okazaki et al. (2015) were collected using the same protocol,
610 which is gentle and rapid melting of surface snow (Duprat et al., 2007; Okazaki et al., 2015).
611 This protocol is specific to these 2 collections, where the particles were trapped in snow at
612 temperatures far below 0 °C before being extracted from their host matrix (the snow) rapidly
613 (within hours). In contrast, MMs from other collections were trapped in a matrix (ice,
614 sediments…) that experienced much larger temperature variations and mechanical stress. In
615 particular, most MMs from the other collections experienced repeated contact with liquid water,
616 in particular during thawing/freezing cycles at the surface of ice fields, whereas the MMs from
617 Dome C and the Dome Fuji samples of Okazaki et al. (2015) experienced only limited contact
618 with liquid water, for a few hours during their extraction (note that this is also different for the
619 samples extracted from snow at Mount Fuji; Osawa et al., 2000; Osawa and Nagao, 2002a).
620 The striking difference in the noble gas concentrations between MMs obtained by different
621 collection methods suggests that part of the noble gases initially present in dust in interplanetary
622 space is hosted by a phase that may be subject to leaching by water.

623 Another interesting feature is the depletion of Xe relative to Kr and the reference CM
624 meteorite ratio (roughly that in phase Q, the major carrier of heavy noble gases in primitive
625 meteorites; Ott, 2014). We have argued previously that this may a sign for contamination by
626 (terrestrial) air, which has an $^{84}Kr/^{132}Xe$ ratio of ~28, much higher than the primitive noble gas
627 component in carbonaceous chondrites (~1). We will come back to this later (chapter 4.3).

628 **4.2. Solar wind gases: Helium and Neon**

629 The solar wind origin of the noble gases He and Ne is highlighted in Figure 6, which is
630 a plot of trapped ^{4}He vs. ^{20}Ne abundances for those AMMs, where both could be measured
631 (Tables 2, 3 and 6). Minor corrections for cosmogenic contributions have been applied but are

negligible. Any radiogenic ^{4}He present is still included, however. Compared to the ^{4}He/^{20}Ne ratio of 656 determined for present-day solar wind (Heber et al., 2009), which defines the solid line in Figure 6, all data points are shifted down / to the right, i.e. have lower ^{4}He/^{20}Ne. As noted before (chapter 4.1; and Baecker et al., 2018), unmelted MMs have higher concentrations of solar wind gases than partially melted (scoriaceous) ones, and the concentrations roughly scale with size, a consequence of the fact that they are surface-correlated. This is also apparent in that MM DC 06_09_11, which is partly scoriaceous (FgC/Sc), has lower concentrations and lower ^{4}He/^{20}Ne than the "purely FgC" MMs. However, we do not observe this for the other FgC/Sc MM DC 06_09_189, which has the highest concentrations of ^{4}He and ^{20}Ne in our sample set.

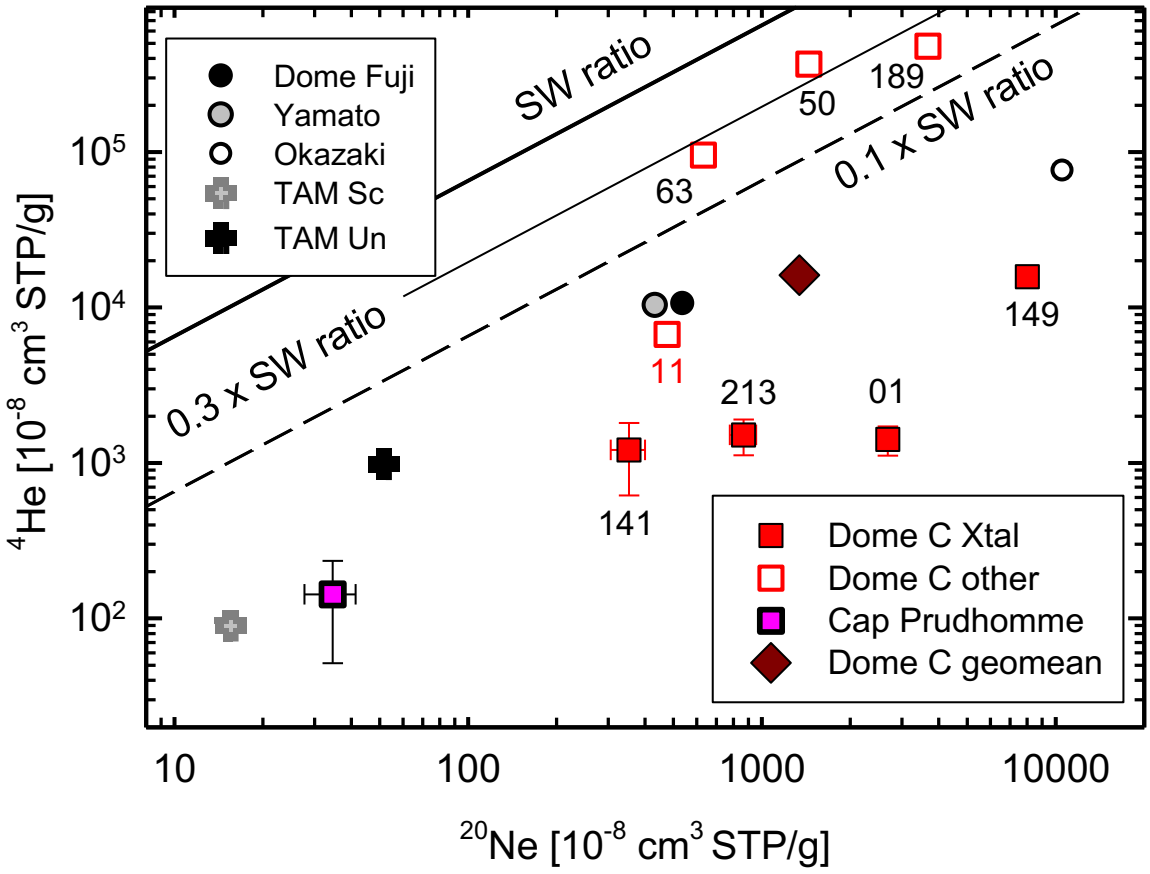

Figure 6: Concentrations of ^{4}He plotted vs. concentrations of trapped ^{20}Ne. The individual data points for our DC MMs are labeled with the last digits of the sample name (Table 1). We also show the geometric means for our DC MMs as well as for the results of previous studies of MMs from Dome Fuji, the Yamato Mountains area and the Transantarctic Mountains. References: Osawa et al. (2000, 2003b), Osawa and Nagao (2002a, b), Baecker et al. (2018). The Dome Fuji value from the Okazaki et al. (2015) study is shown separately, and the TAM MMs are distinguished between Unmelted (Un) and scoriaceous (Sc). The lines correspond to the solar wind ^{4}He/^{20}Ne ratio (Heber et al., 2009), as well as 0.3x and 0.1x the solar wind ratio.

A new feature, not apparent from previous work, is the difference between MMs that are crystalline (Xtal) and those that are fine-grained carbonaceous (FgC). While both cover about the same range in concentrations of Ne, the Xtal ones have significantly lower ^{4}He and thus much lower ^{4}He/^{20}Ne, by almost two orders of magnitude – geometric means are ~1.6 vs. ~170, ignoring partly scoriaceous DC 06_09_11. Previous noble gas studies have mostly distinguished between, on one hand, unmelted (often simply called MM; e.g., Osawa et al., 2003) and, on the other, scoriaceous MMs and completely melted cosmic spherules, thus missing the apparent difference between Xtal and FgC unmelted MMs.

Compared to previous works, the mean ^{4}He and ^{20}Ne concentrations for our Dome C MMs as well as the MMs of Okazaki et al. (2015) are higher, but plot roughly along a line parallel to the solar wind line, i.e. they all have, on average, similar ^{4}He/^{20}Ne ratios, of ~20, i.e. ~0.03 times the SW ratio. On the other hand, our samples clearly defined as FgC MMs, show roughly ten times higher ratios of ~0.3x SW, as do some in the earlier studies (Osawa and Nagao, 2002a; Osawa et al., 2000, 2003b; see also Fig. 2 in Okazaki et al., 2015). The fact that, in all studies so far, the average ^{4}He/^{20}Ne is about the same suggests that, in all these studies, the mix of fine-grained carbonaceous and crystalline MMs was fairly similar.

Interestingly, ^{4}He/^{20}Ne ratios observed in IDPs (Nier and Schlutter, 1990; Pepin et al., 2000) more or less cover the same range as those observed for unmelted MMs. We have argued earlier (Baecker et al., 2018), based on comparison not only with IDPs, but also with lunar soil samples and grains returned from asteroid Itokawa (Nagao et al., 2011), that ratios such as those observed in MMs DC 06_09_50, 06_09_63 and 06_09_189 may be common (characteristic) for the pre-terrestrial ratio in MMs. Even though lower than in solar wind proper, such ratios are therefore not necessarily indicative of loss during passage through the terrestrial atmosphere. Differences in absolute concentrations (of both He and Ne) may then be related to size (via the surface/volume ratio), fractional loss of the outermost ~0.05 nm, where the solar wind gases reside, and - in cases where not the whole MM was used for noble gas analysis - the unknown fraction of surface present in the sample actually used for the noble gas work (Baecker et al., 2018).

As for the difference in average ^{4}He contents and ^{4}He/^{20}Ne ratios between Xtal and FgC MMs, it appears likely that this was established during atmospheric entry heating. The apparent loss of He by one to two orders of magnitude suggested by Fig. 6 is similar to that found by Füri et al. (2013) in their series 1 experiment for two-second heating to 1350 °C of grains of the Orgueil (CI) meteorite, used for simulation of entry heating. After this, the grains were still characterized as fine-grained, non-vesicular (Toppani et al., 2001). We note, however, that in this case Füri et al. (2013) also observed significant loss of Ne (some 80 %), while for our crystalline MMs there is no indication for Ne loss (Fig. 6). We also note that the results of Füri et al. (2013) are compromised by large variations in the abundances of the starting material used for heating and that there is no information on the abundance before heating in the individual samples. In any case, the differences between the Xtal and other grains of our study indicate that, besides the temperature reached during atmospheric entry, the mineralogical makeup of the MM also determines the degree of loss of solar wind He. As a consequence, the temperature dependence of ^{4}He release during analysis (Nier and

Schlutter, 1993; Okazaki et al., 2015) alone may not be a reliable measure for determining the degree of heating experienced by a MM during atmospheric entry.

While in this work on MMs from Dome C we concentrated on unmelted MMs, it useful to keep in mind that even in scoriaceous MMs some solar wind Ne has been retained. Preferred orientation during atmospheric entry that resulted in a small fraction of surface to remain intact may be a possible explanation, but it cannot be excluded that some amount of solar wind gas might have been acquired by subunits of the MMs during residence in an asteroidal regolith prior to assembly and ejection. This could then reside in the MM's interior (Baecker et al., 2018) rather than close to the surface.

4.3. Heavy noble gases: Argon, krypton and xenon

The case of krypton and xenon is distinct from that of He and Ne since they can be expected to be primarily of the "planetary" type (Ott, 2014) and volume- rather than surface-sited. The case of Ar is more complicated and differs from that of our TAM samples (Baecker et al., 2018), since the DC MMs have significantly higher solar wind gases concentrations (chapter 4.2; Figs. 5 and 6).

The difference is also obvious in a plot of $^{36}Ar/^{132}Xe$ vs. $^{84}Kr/^{132}Xe$ (Fig. 7) where the high $^{36}Ar/^{132}Xe$ ratios in all MMs, with the exception 06_09_189, can only be explained by the contribution of solar components. As an example, treating the measured compositions as a 3-component mixture of solar wind, Q and air (all unfractionated), for DC 06_09_63 the contribution to ^{36}Ar of SW is 65% (vs. 24% from air and 11% from Q). For DC 06_09_11, as another example, the corresponding values are 57% (SW), 7% (air) and 35% (Q).

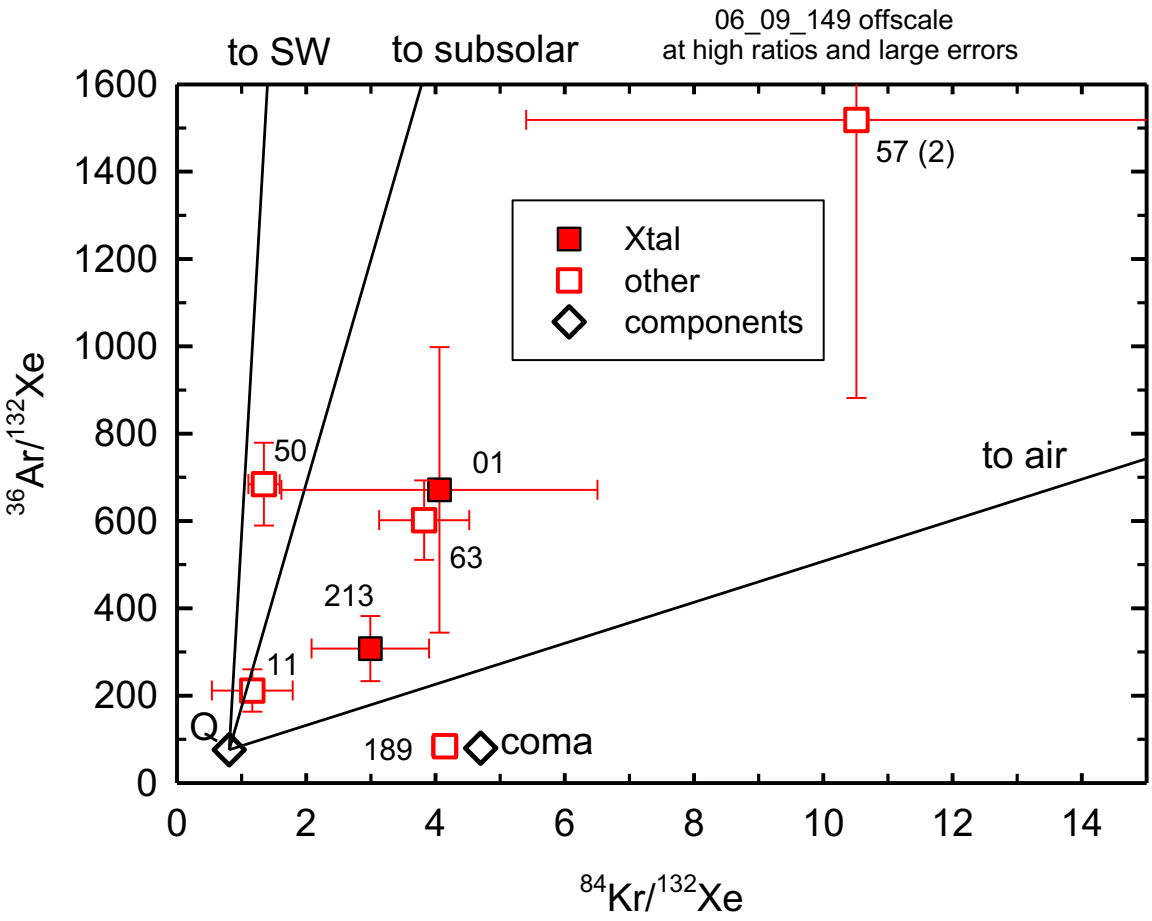

715

716 Figure 7. Plot of $^{36}Ar/^{132}Xe$ vs. $^{84}Kr/^{132}Xe$. The data points are labeled with the last digits of
717 the sample names (Table 1); DC_06_09_149 plots off scale. The composition of Q
718 (Busemann et al., 2000; Ott, 2014) and of gases in the corona of comet Churyumov-
719 Gerasimenko (Rubin et al., 2018) are shown for reference, as well as mixing lines between Q
720 and solar wind (Vogel et al., 2011), subsolar gas (Ott, 2014) and air.

721 On the other hand, it is also obvious, in particular from DC 06_09_11, that a component
722 similar to Q, with low ratios, is needed as well. For Xe, in the three-component mixing model
723 discussed above, Q is always the dominant component, accounting for 88 and 98% in the two
724 examples. As a result, the Xe isotopic compositions discussed in chapters 3.3 and below in
725 chapter 4.5, are essentially those of the non-solar component(s). For Kr, the situation is often
726 not so clear-cut, but from the 3-component exercise it still follows that the SW contribution is
727 comparably small (usually <10%). Of course, the simple 3-component assumption used in the
728 estimates above is somewhat naive, with some of the components being possibly elementally
729 fractionated compared to their normal composition, and with gases that have Ar/Kr/Xe ratios
730 like in the coma of comet Churyumov-Gerasimenko (Rubin et al., 2018) as a possible
731 alternative (to air) or as an additional component. Still, the exercise provides some clues.
732 Interestingly, but possibly just by coincidence, the position of DC 09_06_189 is identical to
733 that of the coma composition. This special MM, which is fine-grained carbonaceous (FgC),
734 but also partially scoriaceous, does not require a contribution from solar wind Ar (nor Kr or
735 Xe, for that matter), which contrasts with the fact that it has the highest abundances of (solar)
736 He and Ne (Fig. 6) and a $^{20}Ne/^{36}Ar$ ratio very much like the others (Table 3).

With SW contributions to Kr probably small (<10%), it makes sense to examine the results for further details (i.e., including concentrations) in the Kr-Xe system alone, which we are doing in Fig. 8. Two of our grains stand out: DC 06_09_189 and the smaller sample from DC 06_09_57. Their concentrations are much higher than those of the Xtal MMs and also in comparison to the other MMs counted among "others". Two of the latter are close in $^{84}Kr/^{132}Xe$ to the ratio in the Q component, indicating little contribution from other components. Overall, these grains have concentrations similar to the MMs from Dome Fuji analyzed by Osawa et al. (2000) and Osawa and Nagao (2002a), which in turn are similar to the most primitive macroscopic meteorites (types 2 and 1). Their concentrations are higher than those of MMs from the Yamato region (Osawa and Nagao, 2002b; Osawa et al. 2003) and from the Transantarctic Mountains (Baecker et al., 2018). There is a clear gap in Fig. 8 between these and the much higher concentrations found in the Dome Fuji samples of Okazaki et al. (2015). Compared to latter, DC 06_09_189 is at the upper end and DC 06_09_57(2) even higher. As discussed above in section 4.1, this striking difference may be related to the specific collection protocol used for the Dome Fuji samples of Okazaki et al. (2015) and our Dome C samples only, and suggests that this specific Kr and Xe component may be hosted by a phase sensitive to repeated episodes of leaching by water. Interestingly, the Ar/Kr/Xe ratio of DC 06_09_189 almost perfectly matches Ar/Kr/Xe in the coma of comet Churyumov-Gerasimenko (Figs. 7, 8). We will come back to this in section 4.5.

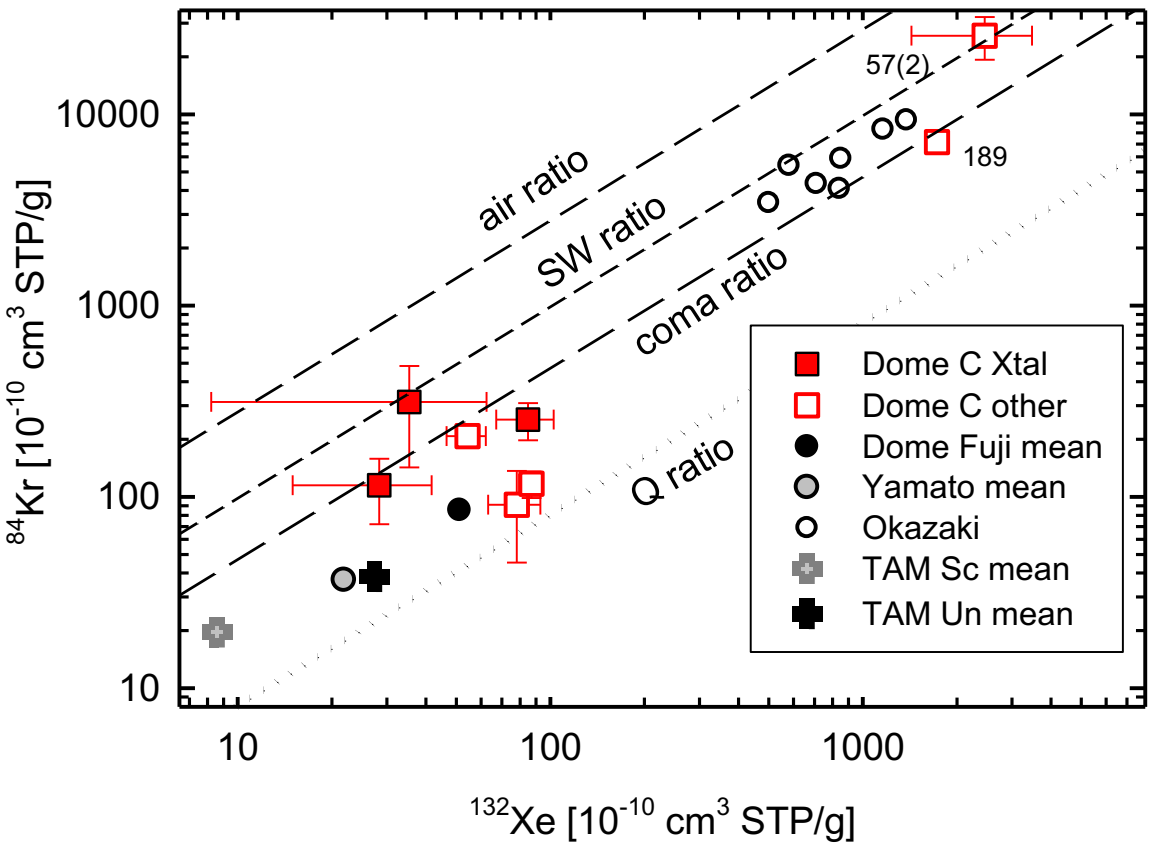

Figure 8. Plot of ^{84}Kr vs. ^{132}Xe concentrations. DC 06_09_189 and DC 06_09_57(2) with the

highest abundances are labeled. For comparison geometric means from previous studies on MMs from Mount Fuji, the Yamato Mountains and the Transantarctic Mountains (TAM) are shown (Osawa et al. ,2000, 2003b; Osawa and Nagao, 2002a, b; Baecker et al. 2018). The Dome Fuji MMs of Okazaki et al. (2015) are shown as individual data points and are not included in the Dome Fuji mean, while the TAM MMs are distinguished between Unmelted (Un) and scoriaceous (Sc). The various lines correspond to the $^{84}Kr/^{132}Xe$ ratio in air, SW, the coma of comet Churyumov-Gerasimenko and Q. References as in Figure 7.

4.4. Cosmic ray exposure (CRE) and provenance

Cosmic ray exposure ages are commonly calculated from the overabundance of isotopes that are much rarer in trapped components than the other isotopes of the same element, but are produced by cosmic ray interaction in roughly equal amounts, such as ^{3}He, ^{21}Ne and ^{38}Ar. Their concentrations – calculated as described in chapter 3.4 - are listed in Table 6. The favored approach is usually that using ^{21}Ne, because this isotope is less susceptible to loss than ^{3}He and less sensitive to variations in chemical composition than ^{38}Ar. The problem in using ^{21}Ne with MMs (as well as IDPs, for that matter) is the high abundance of solar wind Ne (and solar wind He, for the case of ^{3}He). Shifts to the right in the Ne three-isotope plot of Fig. 2 indicative of cosmogenic ^{21}Ne are therefore small and often zero within 2 σ. This is different from the situation in our TAM MMs (Fig. 2), which have generally much lower concentrations of solar wind noble gases (Baecker et al., 2018). It is similar, however, to the situation for MMs from the Yamato Mountains and Dome Fuji (Osawa and Nagao, 2002a, 2002b; Osawa et al., 2000, 2003): no cosmogenic Ne was detected in the Yamato Mountains MMs, and only 10% of the Dome Fuji MMs showed detectable ^{21}Ne excesses (Osawa et al., 2003), mostly such with high $^{20}Ne/^{4}He$ ratios (see their Fig. 5).

From the nominal amounts of cosmogenic ^{21}Ne (Table 6; chapter 3.4), we have calculated nominal cosmic ray exposure ages and inferred places of origin by considering the Poynting-Robertson effect of small particles spiraling towards the Sun (Wyatt and Whipple, 1950; Trappitsch and Leya, 2013). The calculations, the results of which are listed in Table 7, were obtained using the Trappisch and Leya (2013) cosmic ray production rates, with updates. Two values are listed in each case, corresponding to the two approaches for defining the trapped composition used in Table 6 and described in chapter 3.4. We have done the same using ^{3}He (also two sets of values corresponding to the two values in Table 6). For this, we corrected ^{3}He assuming recoil losses of 32% (including losses of directly produced ^{3}He and the larger losses of ^{3}H produced as a precursor), which seems roughly appropriate for particles in the studied size range (Ott et al., 2009; Trappitsch and Leya, 2016). No values are given for the cases (^{21}Ne in DC 06_07_213; ^{3}He in DC 06_09_50 and DC 06_09_149) that result in negative nominal values (see also chapter 4.5). Note also that, apart from the analytical and production rate uncertainties, the action of the Poynting-Robertson effect may be more complicated than in this simple approach, in particular in case of non-spherical and / or fluffy particles (Kimura et al., 2002). Moreover, the approach considers only the Poynting-Robertson effect and not others that may affect the orbit of a particle.

The most convincing case is that of DC 06_08_01, which results in a CRE age of ~2 Ma and a place of origin of ~4 au, i.e. well in the asteroid belt. Notably, ^{3}He gives consistent results, indicating that any loss of cosmogenic ^{3}He has been small. Interestingly, this is an

802 Xtal MM characterized by low concentration of solar wind He, relative to solar wind Ne
803 (chapter 4.2; Fig. 5). On the one hand, the relatively low background of solar wind He leads to
804 a relatively high $^{3}He/^{4}He$ ratio of ~14 x 10^{-4} (Table 2) and thus allows identifying rather
805 clearly the abundance of cosmogenic ^{3}He (Fig. 2). On the other hand, low ^{4}He with high ^{3}He
806 also demonstrates the different loss behavior of surface-sited solar wind vs. cosmogenic He
807 contained in the bulk of the MM. Consistent results from ^{21}Ne and ^{3}He are also obtained for
808 Fg/Sc DC 06_09_11, however with a very short inferred exposure age of only ~0.2 Ma with
809 an origin at ~1.5 au. Ages from ^{21}Ne are also short for DC 06_09_50 and DC 06_09_63,
810 while DC 06_09_189 (Fg/Sc) is similar to DC 06_08_01, i.e. compatible with an origin in the
811 asteroid belt. The same is true for the other case of "safe" cosmogenic ^{3}He, DC _06_07_213
812 (Fig. 1), with an inferred CRE age of ~1 Ma, and coming from ~3 au. No ^{21}Ne age could be
813 obtained for this MM, however. Finally, a rather long cosmic ray exposure from ^{21}Ne is
814 indicated for DC 06_09_149, which has the smallest analytical uncertainty and is clearly
815 offset from the trapped composition lines in Fig. 2. The nominal age of ~15 Ma, still with
816 comparably large uncertainty, suggests an origin at a much larger distance, possibly beyond
817 Saturn, thus from a cometary source. This age (like all the other nominal ages) rests on the
818 assumption that the cosmic ray exposure took place during travel as a small particle.
819 However, it cannot be ruled out that much (or even most) cosmogenic ^{21}Ne production took
820 place in the parent body regolith instead (Trappitsch and Leya, 2013). For GCR production in
821 a well-mixed regolith the ^{21}Ne production rate has been estimated as $0.11x10^{-8}$ cm^3 STP per
822 gram and Ma Trappitsch and Leya, 2013), which in case of DC 06_09_149 would mean an
823 exposure roughly 100 to 150 Ma.

824

Table 7. Nominal cosmic ray exposure (CRE) ages and implied places of origin (distance from the sun) of Dome C MMs. These have been calculated following Trappitsch and Leya (2013) from the interplay between cosmic ray production and action of the Poynting-Robertson effect. The approach assumes ^{21}Ne and ^{3}He excesses over abundances in common trapped components are due to cosmic ray production, as described in the text and listed in Table 6, with an assumed 32% recoil loss of cosmogenic ^{3}He (see text). For production by solar cosmic rays updated production rates for a rigidity of 100 MV have been used. Chemical abundances used for the calculation are CM chondritic. Column 2 gives the type of MM (Table 1). In the calculations masses for the complete MMs three times those of the analyzed specimens were assumed, with correspondingly larger sizes. Values in italics / small print are suspicious and the observed effects may require an explanation other than cosmic ray exposure, as discussed in the text (chapter 4.4).

sample	type	T_{21} (Ma)	r_{21} (au)	T_3 (Ma)	r_3 (au)
DC 06_07_213	Xtal	--	--	1.1 (-0.3, +0.3) 0.9 (-0.3, +0.3)	3.3 (-0.4, +0.4) 3.0 (-0.5, +0.4)
DC 06_08_01	Xtal	2.52 (-1.42, +1.94) 1.50 (-0.89, +1.31)	4.64 (-1.50, +1.46) 3.63 (-1.18, +1.26)	2.1 (-0.3, +0.3) 2.0 (-0.3, +0.3)	4.3 (-0.3, +0.3) 4.1 (-0.3, +0.3)
DC 06_09_11	FgC/Sc	0.20 (-0.13, +0.19) 0.15 (-0.11, +0.18)	1.62 (-0.37, +0.44) 1.50 (-0.34, +0.43)	0.3 (-0.3, +0.7) 0.1 (-0.1, +0.6)	1.9 (-0.9, +1.1) 1.4 (-0.4, +1.2)
DC 06_09_50	FgC	0.11 (-0.06, +0.06) 0.07 (-0.04, +0.04)	1.28 (-0.14, +0.14) 1.17 (-0.09, +0.11)	--	--
DC 06_09_63	FgC/Xtal	0.05 (-0.04, +0.06) 0.03 (-0.03, +0.05)	1.14 (-0.12, +0.14) 1.08 (-0.08, +0.13)	*16.8 (-5.9, +6.0)* *14.7 (-4.0, +4.0)*	*10.2 (-2.0, +1.7)* *9.5 (-1.4, +1.2)*
DC_06_09_149	Xtal	17.2 (-10.3, +10.8) 12.3 (-8.9, +9.9)	14.6 (-5.3, +4.0) 12.4 (-5.8, +4.2)	--	--
DC 06_09_189	FgC/Sc	2.41 (-1.62, +2.35) 1.30 (-0.95, +1.62)	4.78 (-1.93, +1.87) 3.57 (-1.54, +1.67)	*26.1 (-9.2, +9.3)* *16.6 (-14.2, +14.2)*	*15.5 (-3.0, +2.4)* *12.3 (-7.5, +4.5)*

There are several additional results that are difficult to understand (or to accept, for that matter). As for ^{3}He ages, these concern DC 06_09_63 and DC 06_09_189. The latter can be easily explained, though, and will disappear if we allow for a slightly higher ^{3}He/^{4}He ratio for the trapped component (>3.26 x 10^{-4} instead of (2.85 ± 0.12) x 10^{-4} and (3.00 ± 0.20) x 10^{-4} in the two approaches will do). DC 06_09_63 is not as easily explained away. Although the measured ^{3}He/^{4}He of (4.14 ± 0.30) x 10^{-4} is lower than the ratio in the SW proper, it is still much higher than in the FSW component and the mixing approach (alternative 1) suggests a trapped ratio of (2.83 ± 0.40) x 10^{-4}. It is also much higher than in the MMs with the highest SW concentration, where the influence of the cosmogenic component must be suppressed. The lack of equivalent amounts of cosmogenic Ne suggests a non-cosmogenic origin for the ^{3}He (if real), and similarly excesses of ^{3}He not easily attributed to cosmic ray production have been found in some IDPs (Nier and Schlutter, 1993; Pepin et al., 2000, 2001). The more distinct excesses in these studies, with measured ^{3}He/^{4}He often clearly above the SW value, would require unreasonably long CRE times of between 50 Ma and >10 Ga, and are, as in our

852 case, characterized by lack of corresponding excesses of cosmogenic ^{21}Ne. At this time, we
853 cannot add further to the extensive discussions of possible alternative explanations by Pepin et
854 al. (2000, 2001), but none of them seems totally convincing.

855 **4.5. Cometary origins (?)**

856 The smaller IDPs collected in the stratosphere most probably have a cometary origin, in
857 particular for the chondritic porous (CP) subtype (e.g., Bradley, 2005; Ishii et al., 2008;
858 Messenger et al., 2003; Busemann et al., 2009). In contrast, micrometeorites recovered from
859 ice and snow, from traps, or fossil have generally been regarded as of asteroidal origin and as
860 largely related to common meteorites (Kurat et al., 1994; Genge et al., 1997, 2020; Taylor et
861 al., 2012; Cordier and Folco, 2014; Noguchi et al., 2015; Shyam Prasad et al., 2018),
862 including differentiated ones (Taylor et al., 2007; Cordier et al., 2012). The large deuterium
863 excesses (Duprat et al., 2010) and the high nitrogen content of their organic matter (Dartois et
864 al., 2013; Yabuta et al., 2017) is suggestive of a cometary origin for the ultra-carbonaceous
865 MMs, but otherwise the question whether at least some MMs are cometary has loomed large
866 from the start of MM studies (e.g., Noguchi et al., 2015). Still, the modelling by Nesvorný et
867 al. (2010), see also Carrillo-Sánchez et al. (2020) and (Rojas et al, 2021), suggests that a
868 significant part of the cosmic dust reaching Earth in the size range of the MMs may derive
869 from Jupiter Family Comets (JFC).

870 Noble gases can contribute in this matter, in different ways. Particles from asteroidal
871 and cometary sources may have, on average, different entry velocities when encountering
872 Earth, and, in the study of IDPs, Nier and Schlutter (1990, 1993) tried to use the release
873 profile of solar wind He as a measure. In principle, a similar approach might be applicable to
874 MMs, however, as we have shown in chapter 4.1, also the mineralogical makeup plays a role
875 for the observed He abundance: Xtal MMs in our collection have much lower ^{4}He abundances
876 and ^{4}He/^{20}Ne ratios than FgC MMs. While we have not studied the release pattern in this
877 work, presumably it is also different between the two types, which, if not taken into account,
878 tends to obscure the entry effect. Still, it may be a useful approach in future work.

879 Another approach can be based on differences in cosmic ray exposure. In our case, and
880 presumably in all cases involving primitive small particles, this is analytically challenging
881 because of the large abundances of solar wind gas, with only minor and barely (if at all)
882 detectable excesses of cosmogenic ^{3}He and ^{21}Ne, with the added problem that cosmogenic
883 gases (like the trapped gases) may have been lost during atmospheric entry (e.g., Füri et al.,
884 2013; Baecker et al., 2018). In our data set, nominal CRE ages that we were able to obtain are
885 all consistent with an asteroidal source, with the possible exception of DC 06_09_149 and the
886 exception of the possible excess ^{3}He in DC 06_09_63 (chapter 4.4). They do not, however,
887 rule out a cometary origin, as once ejected from their parent body, cometary dust particles are
888 subject to non-gravitational forces that affect their initial velocities and trajectories and may
889 result in orbits close to those expected from asteroidal dust.

890 A third approach can be based on the search for signatures in the trapped noble gas
891 components that have been found in *bona fide* cometary materials. There are two sets of data
892 that we can relate to in this approach, which have sampled different comets (though both

Jupiter Family) and different cometary reservoirs: the mass spectrometer onboard the Rosetta mission measured the composition of noble gases in the coma of comet 67P/Churyumov-Gerasimenko (Marty et al., 2017; Rubin et al., 2018), while He and Ne abundances were measured in the laboratory in solids captured from the coma of 81P/Wild 2 in aerogel and returned to Earth (Marty et al., 2008). The former presumably measured gases that were trapped in ices (maybe primarily CO_2 ice; Rubin et al., 2018), while the latter analysis was of solid particles, probably high-temperature igneous grains (Marty et al., 2008).

In fact, we do find some similarities between the observed signatures, which, however, are suggestive only. Two of our MMs show similarities to features observed in the coma of 67P/Churyumov-Gerasimenko. For one, the elemental abundance ratios $^{36}Ar/^{132}Xe$ and $^{84}Kr/^{132}Xe$ for DC 06_09_189 (Figs. 7 and 8) are almost identical to what has been inferred for the bulk abundance ratios of the coma gases (Rubin et al., 2018). Given that a substantial fraction of ^{36}Ar is probably from solar wind, this must appear to be fortuitous, at least as far as $^{36}Ar/^{132}Xe$ is concerned. One might also expect some elemental fractionation between noble gases trapped in ice vs. other, more refractory, solids.

More telling than elemental ratios are isotopic ratios, and the second similarity is in the isotopic composition of Xe and of Ar. Xe as measured in the coma of Churyumov-Gerasimenko (Marty et al., 2017) is highly diagnostic, i.e. characterized by huge depletions of the two heaviest isotopes, ^{134}Xe and ^{136}Xe, when compared to other Solar System reservoirs. A hint for a contribution from such a component is seen in the Xe pattern of the small MM fraction DC 06_09_57(2) shown in Fig. 4, and in a more extended version in Fig. 9. But this case has been analytically challenging, with an amount of ^{132}Xe of only ~$2x10^{-15}$ cm^3 STP (some 50,000 atoms) after blank correction (^{136}Xe: ~8600 atoms), and where the blank contributed about half of the measured ^{132}Xe (2/3 in case of ^{136}Xe). To illustrate the point, we show in Fig. 9 also the ratios as measured, before blank subtraction. In essence, while suggestive, the measurement errors, both from the MM and Rosetta, are too large for a firm conclusion. It is intriguing, though, that in the same MM sample we also measured highly unusual Ar, with $^{38}Ar/^{36}Ar = 0.1495 \pm 0.039$, significantly lower than in any other well-defined trapped Ar component (chapter 3.2). The corresponding $^{36}Ar/^{38}Ar$ ratio of 6.69 ± 0.17 agrees within uncertainties with the coma $^{36}Ar/^{38}Ar$ ratio of 5.4 ± 1.4 reported by Rubin et al. (2018), however, in this case, the large error of the comet measurement prevents any firm conclusion. In addition, the Ar/Xe and Kr/Xe ratios for DC 06_09_57(2) are significantly larger than reported for coma gas (Fig. 7), so strong elemental fractionation would be required.

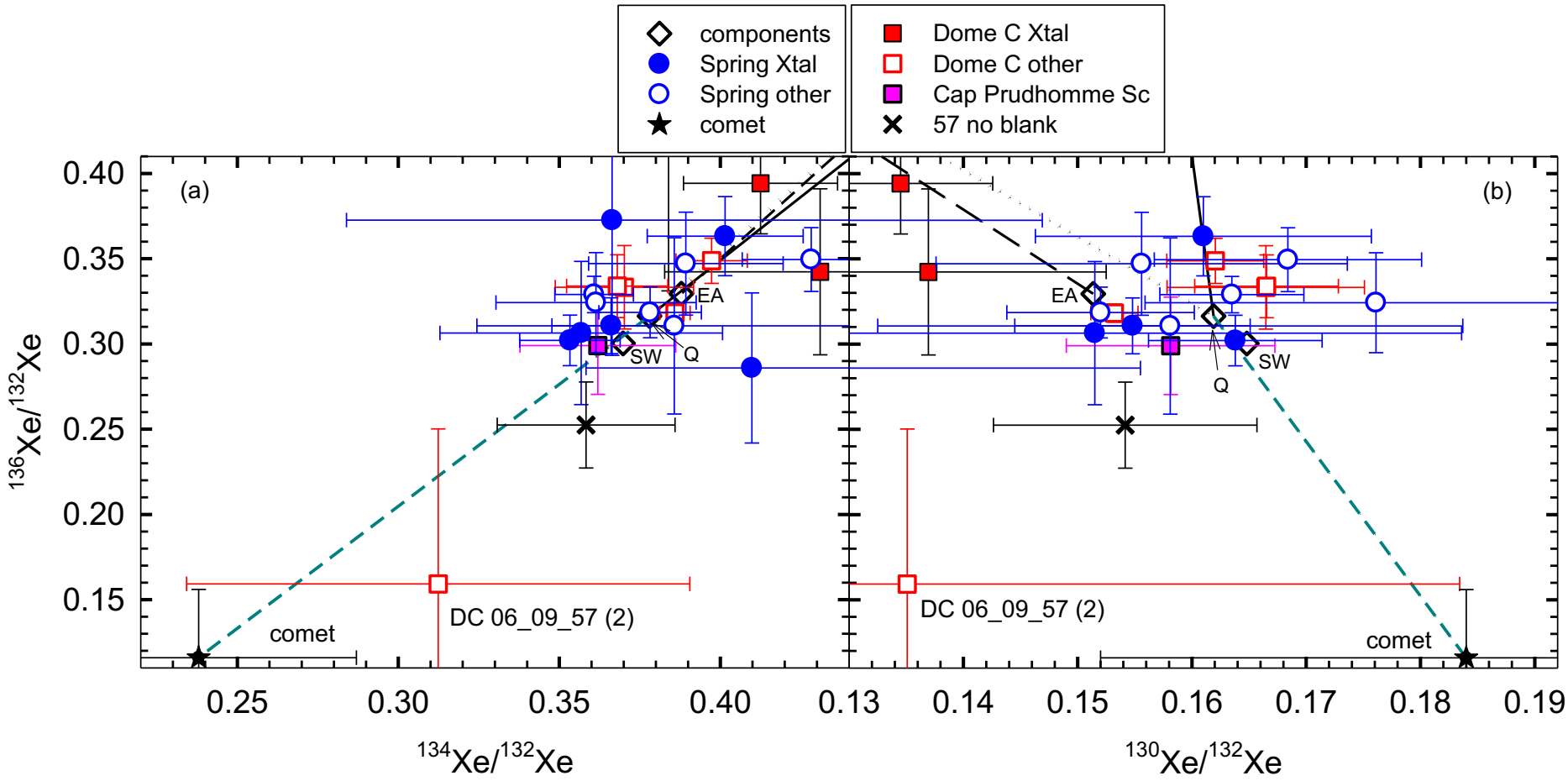

927

928 Figure 9. Same as Figure 4, but with scale expanded to include DC 06_09_57(2) and the composition measured in the coma of comet Churyumov-
929 Gerasimenko (Marty et al., 2017). Also shown is the measured value for DC 06_09_57(2), without extraction blank subtracted ("57 no blank").

930

The signatures discussed above are likely those of the "icy" cometary component, but, in the MMs ,we are dealing with more refractory solids. So, if a connection to our MMs actually exists, there must have been some equilibration between noble gases in cometary ice and cometary solids. Less surprising might be to find, in grains of cometary origin, the signature that has been observed in grains returned by the Stardust mission. The diagnostic feature here is the isotopic composition of Ne, which resembles Ne in the Q phase of chondritic meteorites (Marty et al., 2008). In fact, the same signature appears to have been seen recently in a refractory IDP, Manchanito (Ogliore et al., 2020), for which also other properties point toward a cometary origin. Data for this IDP, as well as the Stardust grain data, are plotted together with our MM data in the Ne three-isotope plot of Fig. 2b. Obviously, two of our Xtal grains, DC 06_07_213 and DC 06_09_141 (both with relatively low ^{20}Ne abundance), plot at a similar position, albeit at slightly higher ^{20}Ne/^{22}Ne, probably due to contribution from SW Ne. Presence of Q as a trapped noble gas component is certainly consistent with the Xe isotopic composition we observe, not only in these, but also most other MMs (Fig. 4; chapter 3.3). but the ^{20}Ne/^{132}Xe ratio for these MMs is on the order of 1000 or higher, i.e. much higher than the ratio of 3 found for Q gas in carbonaceous chondrites (Busemann et al., 2000; Ott, 2014). Thus it is unlikely to be hosted by the Q phase as known from macroscopic meteorites that come from asteroids. It is also opposite the direction expected in case of partial loss of Q-phase noble gases. Obviously, although the analytical errors do not allow to firmly equate the observed composition with that of Q-Ne, the same holds for the Manchanito particle and Stardust grain data. Having data for Xe (or the complete noble gas spectrum) in Manchanito and Stardust grains would have been useful in this context. Still, the similarity between the data is intriguing, and with the Stardust grains undoubtedly cometary, the two MMs and the Manchanito IDP may very well carry cometary signatures.

5. Summary - Conclusions

We have performed a complete noble gas study on fragments from ten Antarctic micrometeorites (AMMs) collected at Dome C, including the isotopes of Kr and Xe, which have been largely missing in previous noble gas studies of micrometeorites. Additional data obtained on a scoriaceous MM from Cap Prudhomme do not provide much information. In the Dome C MMs, He and Ne are dominated by a solar component, with lower ^{4}He concentrations and ^{4}He/^{20}Ne ratios in crystalline (Xtal) compared to fine-grained carbonaceous (FgC) MMs. The latter fall in the high range of solar wind noble gas concentrations seen in earlier work, which may be related to the collection method (gentle and rapid melting of surface snow) and indicate existence of a noble gas host phase in MMs that may be affected by exposure to liquid water. The abundances of (volume-correlated) heavier gases are similar to what was found in previous studies of MMs. For this reason, solar wind is also an important part of Ar and may make also a noticeable contribution to Kr in some cases, however not to Xe.

Xe isotopic ratios are generally in between the composition dominating in primitive macroscopic meteorites (Q component) and air, but, in most cases, uncertainties are too large

for strong conclusions. Because of the high abundances of SW He and Ne, cosmogenic contributions are difficult to resolve. Nevertheless, when resolvable, cosmic ray exposure ages based on cosmogenic ^{21}Ne in combination with the Poynting-Robertson effect are consistent with an origin from the asteroid belt in most cases. The same is true for the rarer cases where we could also derive CRE ages from ^{3}He. One of the MMs (of FgC/Xtal variety) shows a ^{3}He excess similar to what has been seen in some cluster IDPs.

There are hints that some of our (non-representative sample of DC) MMs may relate to a cometary source, but uncertainties are too large for a firm conclusion. These include

- A Xtal MM, for which the abundance of cosmogenic ^{21}Ne suggests it may originate from beyond the orbit of Saturn.
- A small specimen taken from a FgC MM that may contain Xe deficient in the heavy isotopes ^{134}Xe and ^{136}Xe, like in the Xe component identified in the coma of comet 67P/Churyumov-Gerasimenko, where it is probably derived from cometary ice. The same MM has a precisely measured highly unusual ^{36}Ar/^{38}Ar ratio of ~6.7, consistent with the measurement of coma Ar (^{36}Ar/^{38}Ar = 5.4 ± 1.4). In this case, the large error of the coma measurement is an obstacle for a firm conclusion.
- Two MMs of Xtal type, with low SW contributions, that show Ne similar to what has been found in laboratory analysis of refractory grains captured from the coma of comet 81P/Wild 2 by the Stardust mission, and also more recently in the IDP Manchanito, where this was considered as suggesting a cometary origin., While trapped Ne with such a composition is also characteristic of the Q component found in macroscopic meteorites, a connection to Q-Ne (and thus a chondritic parent body) is unlikely because the Ne/Xe ratio (not obtained in the Stardust and Manchanito analyses) differs by orders of magnitude.

Declaration of Competing Interest

The authors declare no competing interests.

Acknowledgments

Siegfried Herrmann and Reinhard Haubold provided technical assistance with noble gas mass spectrometry. B.B., U.O. and M.T. acknowledge funding by the German Research Foundation, DFG-grants OT 171/5-1 and 5-2, M.T. also thanks the Klaus Tschira Stiftung. J.D. and C.E. were financially supported by ANR (Project COMETOR 18-CE31-0011), Region Ile de France (DIM-ACAV+), PNP/INSU, CNES, IN2P3 and Labex P2IO. Collection of the micrometeorites was performed at CONCORDIA Station (project #1120) and financially supported by the French Polar Institute (IPEV). We are grateful to the staff of the French (IPEV) and Italian (PNRA) Polar Institutes for logistical help in the field.

1011

1012

References:

Albarede F., Ballhaus C., Blichert-Toft J., Lee C.-T., Marty B., Moynier F. and Yin Q.-Z. (2013) Asteroidal impacts and the origin of terrestrial and lunar volatiles. *Icarus* **222**, 44-52. https://doi.org/10.1016/j.icarus.2012.10.026.

Alexander C. M. O'D., Bowden R., Fogel M. L., Howard K. T., Herd C. D. K. and Nittler L. R. (2012) The provenances of asteroids, and their contributions to the volatile inventories of the terrestrial planets. *Science* **337**, 721-723. https://doi.org/10.1126/science.1223474.

Baecker B. (2014) Primordial and other noble gases in micrometeorites. PhD Thesis, University of Heidelberg, Germany, 362 p.

Baecker B., Ott U., Cordier C., Folco L., Trieloff M., van Ginneken M. and Rochette P. (2018) Noble gases in micrometeorites from the Transantarctic Mountains. *Geochim. Cosmochim. Acta* **242**, 266-297. https://doi.org/10.1016/j.gca.2018.08.02.

Basford J. R., Dragon J. C., Pepin R. O., Coscio Jr. M. R. and Murthy V. R. (1973) Krypton and xenon in lunar fines. *Proc. 4th Lunar Sci. Conf. (Suppl. 4, Geochim. Cosmochim Acta)*, 1915-1955.

Bekaert D. V., Avice G., Marty B., Henderson B. and Gudipati, M. S. (2017) Stepwise heating of lunar anorthosites 60025, 60215, 65315 possibly reveals an indigenous noble gas component on the Moon. *Geochim. Cosmochim. Acta* **218**, 114-131. https://doi.org/10.1016/j.gca.2017.08.041.

Benkert J.-P., Baur H., Signer P. and Wieler R. (1993) He, Ne, and Ar from the solar wind and solar energetic particles in lunar ilmenites and pyroxenes. *J. Geophys. Res*. **98**, 13,147-13,162. https://doi.org/10.1029/93JE01460.

Bradley J .P. (2005) Interplanetary dust particles. In: Davis, A.M. (Ed.), Treatise in Geo-chemistry, vol.1. Elsevier–Pergamon, Amsterdam, pp.689-711.

Bradley J. P., Ishii H. A., Gillis-Davis J. J., Ciston J., Nielsen M. H., Bechtel H. A. and Martin M. C. (2014) Detection of solar-wind produced water in irradiated rims on silicate minerals. *Proc. Natl. Acad. Sci.* **111**, 1732-1735. https://doi.org/10.1073/pnas.132011511.

Britt D. and Consolmagno G. (2003) Stony meteorite porosities and densities: A review of the data through 2001. *Meteoritics & Planetary Science* **38**, 1161-1180. https://doi.org/10.1111/j.1945-5100.2003.tb00305.x.

Busemann H., Baur H. and Wieler R. (2000) Primordial noble gases in "phase Q" in carbonaceous and ordinary chondrites studied by closed system stepped etching. *Meteorit. Planet. Sci.* **35**, 949-973. https://doi.org/10.1111/j.1945-5100.2000.tb01485.x.

Busemann H., Nguyen A. N., Cody G. D., Hoppe P., Kilcoyne A. L. D., Stroud R. M., Zega T. J. and Nittler L. R. (2009) Ultra-primitive interplanetary dust particles from the

comet 26P/Grigg–Skjellerup dust stream collection. *Earth Planet. Sci. Lett.* **288**, 44–57. https://doi.org/10.1016/j.epsl.2009.09.007.

Carillo-Sánchez J. D., Gómez-Martin H. C., Bones D. L., Nesvorný D., Pokorný P., Benna M., Flynn G. J. and Plane J.M.C. (2020) Cosmic dust fluxes in the atmospheres of Earth, Mars, and Venus. *Icarus* **335**, #113395. https://doi.org/10.1016/j.icarus.2019.113395.

Cartwright J. A., Ott U., Herrmann S. and Agee C. B. (2014) Modern atmospheric signatures in 4.4 Ga Martian meteorite NWA 7034. *Earth Planet. Sci. Lett.* **400**, 77-87. https://doi.org/10.1016/j.epsl.2014.05.008.

Cordier C. and Folco L. (2014) Oxygen isotopes in cosmic spherules and the composition of the near Earth interplanetary dust complex. *Geochim. Cosmochim. Acta* **146**, 18-26. https://doi.org/10.1016/j.gca.2014.09.038.

Cordier C., Folco L., Suavet C., Sonzogni C. and Rochette P. (2011a) Major, trace element and oxygen isotope study of glass cosmic spherules of chondritic composition: The record of their source material and atmospheric entry heating. *Geochim. Cosmochim. Acta* **75**, 5203-5218. https://doi.org/10.1016/j.gca.2011.06.014.

Cordier C., Folco L. and Taylor S. (2011b) Vestoid cosmic spherules from the South Pole Water Well and Transantarctic Mountains (Antarctica): A major and trace element study. *Geochim. Cosmochim. Acta* **75**, 1199-1215. https://doi.org/10.1016/j.gca.2010.11.024.

Cordier C., Suavet C., Folco L., Rochette P. and Sonzogni C. (2012) HED-like cosmic spherules from the Transantarctic Mountains, Antarctica: Major and trace element abundances and oxygen isotopic compositions. *Geochim. Cosmochim. Acta* **77**, 515-529. https://doi.org/10.1016/j.gca.2011.10.021.

Cordier C., Baecker B., Ott U., Folco L. and Trieloff M. (2018) A new type of oxidized and pre-irradiated micrometeorite. *Geochim. Cosmochim. Acta* ***233***, 135-158. https://doi.org/10.1016/j.gca.2018.04.010.

Cremonese G., Borin P., Martellato E., Marzari F. and Bruno M. (2012) New calibration of the micrometeoroid flux on Earth. *Astrophys. J. Lett.* **749**, L40. https://doi.org/10.1088/2041-8205/749/2/L40.

Crowther S., Mohapatra R. K., Turner G., Blagburn D., Kehm K., and Gilmour J. D. (2008) Characteristics and applications of RELAX, an ultrasensitive resonance ionization mass spectrometer for xenon. *J. Anal. At. Spectrom.* **23**, 938-947. https://doi.10.1039/B802899K.

Dartois E., Engrand C., Brunetto R., Duprat J., Pino T., Quirico E., Remusat L., Bardin N., Briani G., Mostefaoui S., Morinaud G., Crane B., Szwec N., Delauche L., Jamme F., Sandt Ch. and Dumas P. (2013) UltraCarbonaceous Antarctic micrometeorites, probing the Solar System beyond the nitrogen snow-line. *Icarus* **224**, 243-252. https://doi.org/10.1016/j.icarus.2013.03.002.

1089 Dartois E., Engrand C., Duprat J., Godard M., Charon E., Delauche L., Sandt C. and
1090 Borondics F. (2018) Dome C ultracarbonaceous Antarctic micrometeorites. Infrared and
1091 Raman fingerprints. *Astron. Astrophys.* **609**, A65. https://doi:10.1051/0004-
1092 6361/201731322.

1093 Duprat J., Engrand C., Maurette M., Kurat G., Gounelle M. and Hammer C. (2007)
1094 Micrometeorites from central Antarctic snow: The CONCORDIA collection. *Adv.Space*
1095 *Res.* **39**, 605-611. https://doi.org/10.1016/j.asr.2006.05.029.

1096 Duprat J., Dobricâ E., Engrand C., Aléon J., Marrocchi Y., Mostefaoui S., Meibom A.,
1097 Leroux H., Rouzaud J.-N. and Gounelle M. (2010) Extreme Deuterium excesses in
1098 ultracarbonaceous micrometeorites from Central Antarctic snow. *Science* **328**, 742-
1099 745. https://doi.org/10.1126/science.1184832.

1100 Eberhardt P., Eugster O., and Marti K. (1965) A redetermination of the isotopic composition
1101 of atmospheric neon. *Z. Naturforsch.* **20a**, 623-624. https://doi.org/10.1515/zna-1965-
1102 0420.

1103 Engrand C. and Maurette M. (1998) Carbonaceous micrometeorites from Antarctica.
1104 *Meteorit. Planet. Sci.* **33**, 565-580. https://doi.org/10.1111/j.1945-5100.1998.tb01665.x.

1105 Flynn G. J. (1996) The delivery of organic matter from asteroids and comets to the early
1106 surface of Mars. *Earth, Moon, and Planets* **72**, 469-474.
1107 https://doi.org/10.1007/BF00117551.

1108 Folco L., Rochette P., Perchiazzi N., D'Orazio M., Laurenzi M. A. and Tiepolo M. (2008)
1109 Microtektites from Victoria Land Transantarctic Mountains. *Geology* **36**, 291-294.
1110 https://doi.org/10.1130/G24528A.1.

1111 Füri E., Aléon-Toppani A., Marty B., Libourel G. and Zimmermann L. (2013) Effects of
1112 atmospheric entry heating on the noble gas and nitrogen content of micrometeorites.
1113 *Earth Planet. Sci. Lett.* **377-378**, 1-12. https://doi.org/10.1016/j.epsl.2013.07.031.

1114 Gardner C. S., Liu A. Z., Marsh D. R., Feng W. and Plane J. M. C. (2014) Inferring the
1115 global cosmic dust influx to the Earth's atmosphere from lidar observations of the
1116 vertical flux of mesospheric Na. *J. Geophys. Res. Space Physics* **119**, 7870–7879.

1117 Genge M. J. (2008) Micrometeorites and their implications for meteors. *Earth, Moon, and*
1118 *Planets* **102**, 525-535. https://doi.org/10.1007/s11038-007-9185-z.

1119 Genge M. J., Grady M. M. and Hutchison R. (1997) The textures and compositions of fine-
1120 grained Antarctic micrometeorites: Implications for comparison with meteorites.
1121 *Geochim. Cosmochim. Acta* ***61***, 5149-5162. https://doi.org/10.1016/S0016-
1122 7037(97)00308-6.

1123 Genge M. J., Engrand C., Gounelle M. and Taylor S. (2008) The classification of
1124 micrometeorites. *Meteorit. Planet. Sci.* **43**, 497-515. https://doi.org/10.1111/j.1945-
1125 5100.2008.tb00668.x

1126 Genge, M. J., van Ginneken M., Suttle M. D. and Harvey R.P. (2018) Accumulation
1127 mechanisms of micrometeorites in an ancient supraglacial moraine at Larkman
1128 Nunatak, Antarctica. *Meteorit. Planet. Sci.* **53**, 2051-2066.
1129 https://doi.org/10.1111/maps.13107.

1130 Genge M. J., Van Ginneken M. and Suttle M. D. (2020) Micrometeorites: Insights into the
1131 flux, sources and atmospheric entry of extraterrestrial dust at Earth. *Planetary and Space*
1132 *Science* **187**, #104900. https://doi.org/10.1016/j.pss.2020.104900.

1133 Gilmour J. D., Lyon I. C., Johnston W. A. and Turner G. (1994) RELAX: An ultrasensitive,
1134 resonance ionization mass spectrometer for xenon. *Rev. Sci. Instr.* **65**, 617-625.
1135 https://doi.org/10.1063/1.1145127.

1136 Grün E., Zook H. A., Fechtig H. and Giese R. H. (1985) Collisional balance of the meteoritic
1137 complex. *Icarus* **62**, 244–272. https://doi.org/10.1016/0019-1035(85)90121-6.

1138 Haack H., Grau T., Bischoff A., Horstmann M., Wasson J. T., Sørensen A., Laubenstein M.,
1139 Ott U., Palme H., Gellissen M., Greenwood R. C., Pearson V. K., Franchi I. A., Gabelica
1140 Z. and Schmitt-Kopplin P. (2012) Maribo-A new CM fall from Denmark. *Meteorit.*
1141 *Planet. Sci.* **47**, 30–50. https://doi.org/10.1111/j.1945-5100.2011.01311.x.

1142 Heber V. S., Wieler R., Baur H., Olinger C., Friedmann T. A. and Burnett D. S. (2009) Noble
1143 gas composition of the solar wind as collected by the Genesis mission. *Geochim.*
1144 *Cosmochim. Acta* **73**, 7414-7432. https://doi.org/10.1016/j.gca.2009.09.013.

1145 Heber V. S., Baur H., Bochsler P., McKeegan K. D., Neugebauer M., Reisenfeld D. B.,
1146 Wieler R. and Wiens R. C. (2012) Isotopic Mass Fractionation of Solar Wind: Evidence
1147 from fast and slow Solar Wind collected by the Genesis mission. *Astrophy. J.* **759**, 121.
1148 https://doi.org/10.1088/0004-637X/759/2/121.

1149 Hébrard E. and Marty B. (2014) Coupled noble gas-hydrocarbon evolution of the early Earth
1150 atmosphere upon solar UV irradiation. *Earth Planet. Sci. Lett.* **385**, 40-48.
1151 https://doi.org/10.1016/j.epsl.2013.10.022.

1152 Huss G. R. and Lewis R. S. (1994) Noble gases in presolar diamonds I: Three distinct
1153 components and their implications for diamond origins. *Meteoritics* **29**, 791-810.
1154 https://doi.org/10.1111/j.1945-5100.1994.tb01094.x.

1155 Imae N., Taylor S. and Iwata N. (2013) Micrometeorite precursors: Clues from the
1156 mineralogy and petrology of their relict minerals. *Geochim. Cosmochim. Acta* **100**, 116-
1157 157. https://doi.org/10.1016/j.gca.2012.09.052.

1158 Ishii H. A., Bradley J. P., Dai Z. R., Chi M., Kearsley A. T., Burchell M. J., Browning N. D.,
1159 and Molster F. (2008) Comparison of comet 81P/Wild 2 dust with interplanetary dust
1160 from comets. *Science* **319**, 447–450. https://doi.org/10.1126/science.1150683.

1161 Kimura, H., Okamoto, H. and Mukai, T. (2002) Radiation pressure and the Poynting-
1162 Robertson effect for fluffy dust particles. *Icarus* **157**, 349–361.
1163 https://doi.org/10.1006/icar.2002.6849.

Kurat G., Koeberl C., Presper T., Brandstätter F. and Maurette M. (1994) Petrology and geochemistry of Antarctic micrometeorites. *Geochim. Cosmochim. Acta* **58**, 3879-3904. https://doi.org/10.1016/0016-7037(94)90369-7

Lee J. Y., Marti K., Severinghaus J. P., Kawamura K., Yoo H. S., Lee J. B. and Kim J. S. (2006) A redetermination of the isotopic abundances of atmospheric Ar. *Geochim. Cosmochim. Acta* **70**, 4507-4512. https://doi.org/10.1016/j.gca.2006.06.1563.

Love S. G and Brownlee D. E. (1993) A direct measurement of the terrestrial mass accretion rate of cosmic dust. *Science* **262**, 550-553. https://doi.org/10.1126/science.262.5133.550.

Marty B. (2012) The origins and concentrations of water, carbon, nitrogen and noble gases on Earth. *Earth Planet. Sci. Lett.* **313-314**, 56-66. https://doi.org/10.1016/j.epsl.2011.10.040.

Marty B., Matrajt G., Zimmermann L., Engrand C. and Duprat J. (2002) Nitrogen and noble gas isotopes in Antarctic micrometeorites. *Lunar Planet. Sci.* **33**, abstract #1578.

Marty B., Robert P. and Zimmermann L. (2005) Nitrogen and noble gases in micrometeorites. *Meteorit. Planet. Sci.* **40**, 881-894. https://doi.org/10.1111/j.1945-5100.2005.tb00161.x.

Marty B., Palma R. L., Pepin R. O., Zimmermann L., Schlutter D. J., Burnard P. G., Westphal A. J., Snead C. J., Bajt S., Becker R. H. and Simones J. E. (2008) Helium and neon abundances and compositions in cometary matter. *Science* **319**, 75-78. https://doi.org/10.1126/science.1148001.

Marty B., Avice G., Sano Y., Altwegg K., Balsiger H., Hässig M., Morbidelli A., Mousis O. and Rubin M. (2016) Origins of volatile elements (H, C, N, noble gases) on Earth and Mars in light of recent results from the ROSETTA cometary mission. *Earth Planet. Sci. Lett.* **441**, 91-102. https://doi.org/10.1016/j.epsl.2016.02.031.

Marty B., Altwegg K., Balsiger H., Bar-Nun A., Bekaert D. V., Berthelier J.-J., Bieler A., Briois C., Calmonte U., Combi M., De Keyser J., Fiethe B., Fuselier S. A., Gasc S., Gombosi T. I., Hansen K. C., Hässig M., Jäckel A., Kopp E., Korth A., Le Roy L., Mall U., Mousis O., Owen T., Rème H., Rubin M., Sémon T., Tzou C.-Y., Waite J. H. and Wurz P. (2017) Xenon isotopes in 67P/Churyumov-Gerasimenko show that comets contributed to Earth's atmosphere. *Science* **356**, 1069-1072. https://doi.org/10.1126/science.aal3496.

Maurette M. (2006) Micrometeorites and the Mysteries of Our Origins. Springer-Verlag, Berlin Heidelberg, New York, 330 pp..

Maurette M., Olinger C., Christophe Michel-Levy M., Kurat G., Pourchet M., Brandstätter F. and Bourot-Denise M. (1991) A collection of diverse micrometeorites recovered from 100 tonnes of Antarctic blue ice. *Nature* **351**, 44-47. https://doi.org/10.1038/351044a0.

Maurette M., Duprat J., Engrand C., Gounelle M., Kurat G., Matrajt G. and Toppani A. (2000) Accretion of neon, organics, CO_2, nitrogen and water from large interplanetary dust particles on the early Earth. *Planet. Space Sci.* **48**, 1117-1137. https://doi.org/10.1016/S0032-0633(00)00086-6.

Meshik A., Hohenberg C., Pravdivtseva O. and Burnett D. (2014) Heavy noble gases in solar wind delivered by Genesis mission. *Geochim. Cosmochim. Acta* **127**, 326-347. https://doi.org/10.1016/j.gca.2013.11.030.

Meshik A. P., Pravdivtseva O. V., Hohenberg C. M. and Burnett D. S. (2015) Refined composition of solar wind xenon delivered by Genesis: Implication for primitive terrestrial xenon. *Lunar Planet Sci.* **46**, #2640 (abstract).

Messenger S., Keller L. P., Stadermann F. J., Walker R. M. and Zinner E. (2003) Samples of stars beyond the solar system: silicate grains in interplanetary dust. *Science* **300**, 105–108. https://doi.org/10.1126/science.1080576.

Nagao K., Okazaki R., Nakamura T., Miura Y. N., Osawa T., Bajo K.-i., Matsuda S., Ebihara M., Ireland T. R., Kitajima F., Naraoka H., Noguchi T., Tsuchiyama A., Yurimoto H., Zolensky M. E., Uesugi M., Shirai K., Abe M., Yada T., Ishibashi Y., Fujimura A., Mukai T., Ueno M., Okada T., Yoshikawa M. and Kawaguchi J. (2011) Irradiation history of Itokawa regolith material deduced from noble gases in the Hayabusa samples. *Science* **333**, 1128-1131. https://doi.org/10.1126/science.1207785.

Nakamura T., Noguchi T., Ozono Y., Osawa T. and Nagao K. (2005) Mineralogy of ultracarbonaceous large micrometeorites. *68th Annu. Meteorit. Soc. Meeting*, abstract #5046.

Nesvorný D., Jenniskens P., Levison H. F., Bottke W. F., Vokrouhlický D. and Gounelle M. (2010) Cometary origin of the Zodiacal Cloud and carbonaceous micrometeorites. Implications for hot debris disks. *Astrophys. Journ.* **713**, 816-836. https://doi.org/10.1088/0004-637X/713/2/816.

Nier A. O. and Schlutter D. J. (1990) Helium and neon isotopes in stratospheric particles. *Meteoritics* **25**, 263–267. https://doi.org/10.1111/j.1945-5100.1990.tb00710.x.

Nier A. O. and Schlutter D. J. (1993) The thermal history of interplanetary dust particles collected in the Earth's stratosphere. *Meteoritics* **28**, 675-681. https://doi.org/10.1111/j.1945-5100.1993.tb00639.x.

Noguchi T., Ohashi N., Tsujimoto S., Mitsunari T., Bradley J. P., Nakamura T., Toh S., Stephan T., Iwatag N., and Imae N. (2015) Cometary dust in Antarctic ice and snow: Past and present chondritic porous micrometeorites preserved on the Earth's surface. *Earth Planet. Sci. Lett.* **410**, 1-11. https://doi.org/10.1016/j.epsl.2014.11.012.

Ogliore R. C., Palma R. L., Stodolna, J., Nagashima K., Pepin R. O., Schlutter D. J., Gainsforth Z., Westphal A. J. and Huss G. R. (2020) Q-Gases in a late-forming refractory interplanetary dust particle: A link to comet Wild 2. *Geochim. Cosmochim. Acta* **271**, 116-131. https://doi.org/10.1016/j.gca.2019.11.033.

1240 Okazaki R., Noguchi T., Tsujimoto S.-i., Tobimatsu Y., Nakamura T., Ebihara M., Itoh S.,
1241 Nagahara H., Tachibana S., Terada K. and Yabuta H. (2015) Mineralogy and noble gas
1242 isotopes of micrometeorites collected from Antarctic snow. *Earth, Planets and Space* **67**,
1243 90. https://doi.org/10.1186/s40623-015-0261-8.

1244 Olinger C. T., Maurette M., Das J. P. and Meshik A. (2013) Noble gas contents of unmelted
1245 Cap-Prudhomme "Giant Micrometeorites". *Lunar Planet. Sci.* **44**, abstract #2278.

1246 Osawa T. and Nagao K. (2002a) Noble gas compositions of Antarctic micrometeorites
1247 collected at the Dome Fuji station in 1996 and 1997. *Meteorit. Planet. Sci.* **37**, 911–936.
1248 https://doi.org/10.1111/j.1945-5100.2002.tb00867.x.

1249 Osawa T. and Nagao K. (2002b) On low noble gas concentrations in Antarctic
1250 micrometeorites collected from Kuwagata Nunatak in the Yamato meteorite ice field.
1251 *Antarct. Meteorite Res.* **15**, 165-177.

1252 Osawa T., Nagao K., Nakamura T. and Takaoka N. (2000) Noble gas measurement in
1253 individual micrometeorites using laser gas-extraction system. *Antarct. Meteorite Res.* **13**,
1254 322-341.

1255 Osawa T., Nagao K., Noguchi T., Nakazawa A. and Mikada J. I. (2003a) Remnant
1256 extraterrestrial noble gases in Antarctic cosmic spherules. *Antarct. Meteorite Res.* **16**,
1257 196-219.

1258 Osawa T., Nakamura T. and Nagao K. (2003b) Noble gas isotopes and mineral assemblages
1259 of Antarctic micrometeorites collected at the meteorite ice field around the Yamato
1260 Mountains. *Meteorit. Planet. Sci.* **38**, 1627–1640. https://doi.org/10.1111/j.1945-
1261 5100.2003.tb00005.x.

1262 Osawa T., Yamamoto Y., Noguchi T., Iose A. and Nagao K. (2010) Interior textures,
1263 chemical compositions, and noble gas signatures of Antarctic cosmic spherules: Possible
1264 sources of spherules with long exposure ages. *Meteorit. Planet. Sci.* **45**, 1320-1339.
1265 https://doi.org/10.1111/j.1945-5100.2010.01093.x.

1266 Ott U. (2014) Planetary and pre-solar noble gases in meteorites. *Chemie der Erde –*
1267 *Geochem.* **74**, 519-544. https://doi.org/10.1016/j.chemer.2014.01.003.

1268 Ott U. and Begemann F. (1985) Are all the Martian meteorites from Mars? *Nature* **317**, 509-
1269 512. https://doi.org/10.1038/317509a0.

1270 Ott U., Heck P. R., Gyngard F., Wieler R., Wrobel F., Amari S. and Zinner E. (2009) He and
1271 Ne ages of large presolar silicon carbide grains: Solving the recoil problem. *Pub.*
1272 *Astronom. Soc. Australia* **26**, 297–302. https://doi:10.1071/AS08039.

1273 Ott U., Swindle T. D. and Schwenzer S. P. (2019) Noble gases in Martian meteorites:
1274 Budget, sources, sinks, and processes, In: *Volatiles in the Martian Crust* (ed. J. Filiberto
1275 and S.P. Schwenzer), 35-70, Elsevier.

1276 Owen T. (2008) The contributions of comets to planets, atmospheres, and life: Insights from
1277 Cassini-Huygens, Galileo, Giotto and inner planet missions. *Space Sci. Rev.* **138**, 301-
1278 316. https://doi.org/10.1007/s11214-008-9306-7.

1279 Owen T. and Bar-Nun A. (1993) Noble gases in atmospheres. *Nature* **361**, 693-694.

1280 Owen T., Bar-Nun A. and Kleinfeld I. (1992) Possible cometary origin of heavy noble gases
1281 in the atmospheres of Venus, Earth and Mars. *Nature* **358**, 43-46.
1282 https://doi.org/10.1038/358043a0.

1283 Ozima M. and Podosek F. A. (2002) Noble Gas Geochemistry. Cambridge University Press,
1284 Cambridge, New York, Oakleigh, Madrid, Cape Town. 286 pp..

1285 Pepin R. O. (1991) On the origin and early evolution of terrestrial planet atmospheres and
1286 meteoritic volatiles. *Icarus* **92**, 2-79. https://doi.org/10.1016/0019-1035(91)90036-S.

1287 Pepin R. O. (2006) Atmospheres on the terrestrial planets: Clues to origin and evolution.
1288 *Earth Planet. Sci. Lett.* **252**, 1-14. https://doi.org/10.1016/j.epsl.2006.09.014.

1289 Pepin R. O. and Porcelli D. (2002) Origin of noble gases in the terrestrial planets. In: *Noble*
1290 *Gases in Geochemistry and Cosmochemistry* (eds. D. Porcelli, C. J. Ballentine and R.
1291 Wieler). *Rev. Min. Geochem.* **47**, 191-246. https://doi.org/10.2138/rmg.2002.47.7.

1292 Pepin R. O., Palma R. L. and Schlutter D. J. (2000) Noble gases in interplanetary dust
1293 particles, I: The excess helium-3 problem and estimates of the relative fluxes of solar
1294 wind and solar energetic particles in interplanetary space. *Meteorit. Planet. Sci.* **35**, 495-
1295 504. https://doi.org/10.1111/j.1945-5100.2000.tb01431.x.

1296 Pepin R. O., Palma R. L. and Schlutter D. J. (2001) Noble gases in interplanetary dust
1297 particles, II: Excess helium-3 in cluster particles and modeling constraints on
1298 interplanetary dust particle exposure to cosmic-ray irradiation. *Meteorit. Planet. Sci.* **36**,
1299 1515-1534. https://doi.org/10.1111/j.1945-5100.2001.tb01843.x.

1300 Pernet-Fisher J. F., Joy K. H. and Gilmour J. D. (2020) Identifying primitive noble gas
1301 components in lunar ferroan anorthosites. *Icarus* **352**, 113977.
1302 https://doi.org/10.1016/j.icarus.2020.113977.

1303 Piani L., Marrocchi Y., Rigaudier T., Vacher L. G., Thomassin D. and Marty B. (2020)
1304 Earth's water may have been inherited from material similar to enstatite chondrite
1305 meteorites. *Science* **369**, 1110-1113. https://doi.org/10.1126/science.aba1948.

1306 Rochette P., Folco L., Suavet C., van Ginneken M., Gattacceca J., Perchiazzi N., Braucher R.
1307 and Harvey R. P. (2008) Micrometeorites from the Transantarctic Mountains. *Proc.*
1308 *National Acad. Sci.* **105**, 18206-18211. https://doi.org/10.1073/pnas.0806049105.

1309 Rojas J., Duprat J., Engrand C., Dartois E., Delauche L., Godard M., Gounelle M., Carrillo-
1310 Sánchez J. D., Pokorný P. and Plane J. M. C. (2021) The micrometeorite flux at Dome
1311 C (Antarctica), monitoring the accretion of extraterrestrial dust on Earth. *Earth Planet.*
1312 *Sci. Lett.* **560**, # 116794. https://doi.org/10.1016/j.epsl.2021.116794.

1313 Rubin M., Altwegg K., Balsiger H., Bar-Nun A., Berthelier J.-J., Briois C., Calmonte U.,
1314 Combi M., De Keyser J., Fiethe B., Fuselier S. A., Gasc S., Gombosi T. I., Hansen K.
1315 C., Kopp E., Korth A., Laufer D., Le Roy L., Mall U., Marty B., Mousis O., Owen T.,
1316 Rème H., Sémon T., Tzou C.-Y., Waite J. H. and Wurz P. (2018) Krypton isotopes and
1317 noble gas abundances in the coma of 67/PChuryumov-Gerasimenko. *Science Advances*
1318 **4,** eaar6297. https://doi.org/10.1126/sciadv.aar6297.

1319 Sarda Ph., Staudacher Th. and Allègre C. J. (1991) Complete rare gas study of a very large
1320 unmelted cosmic dust particle from Greenland. *Lunar Planet. Sci.* **22**, 1165-1166
1321 (abstract).

1322 Schmitz B., Feist R., Meier M. M .M., Martin E., Heck P. R, Lenaz D., Topa D., Busemann
1323 H., Maden C., Plant A. A. and Terfelt F. (2019) The micrometeorite flux to Earth
1324 during the Frasnian–Famennian transition reconstructed in the Coumiac GSSP section,
1325 France. *Earth Planet. Sci. Lett.* **522**, 234-243.
1326 https://doi.org/10.1016/j.epsl.2019.06.025.

1327 Schwenzer S. P., Herrmann S., Mohapatra R. K. and Ott U. (2007) Noble gases in mineral
1328 separates from three shergottites: Shergotty, Zagami, and EETA79001. *Meteorit.*
1329 *Planet. Sci.* **42**, 387-412. https://doi.org/10.1111/j.1945-5100.2007.tb00241.x.

1330 Shyam Prasad M., Rudraswami N. G., de Araujo A. A. and Khedekar V. D. (2018)
1331 Characterisation, sources and flux of unmelted micrometeorites on Earth during the last
1332 ~50,000 Years. *Scientific Reports* **8**, 8887. https://doi.org/10.1038/s41598-018-27158-x.

1333 Spring N. H. (2014) Investigating the Origin and Distribution of Primordial Noble Gases and
1334 Volatiles in Asteroids and Comets: A Comparative Study of Interplanetary Dust Particles
1335 (IDPs), Antarctic Micrometeorites (AMMs) and Carbonaceous Chondrites. PhD Thesis.
1336 *University of Manchester, United Kingdom*, 178 p.

1337 Stuart F., Harrop P. J., Knott S., and Turner G. (1999) Laser extraction of helium isotopes
1338 from Antarctic micrometeorites: Source of He and implications for the flux of
1339 extraterrestrial ^{3}He to earth. *Geochim. Cosmochim. Acta* **63**, 2653-2665.
1340 https://doi.org/10.1016/S0016-7037(99)00161-1.

1341 Suavet C., Cordier C., Rochette P., Folco L., Gattacceca J., Sonzogni C. and Damphoffer D.
1342 (2011) Ordinary chondrite-related giant (> 800µm) cosmic spherules from the
1343 Transantarctic Mountains, Antarctica. *Geochim. Cosmochim. Acta* **75**, 6200-6210.
1344 https://doi.org/10.1016/j.gca.2011.07.034.

1345 Suttle, M. D. and Folco L. (2020) The extraterrestrial dust flux: Size distribution and mass
1346 contribution estimates inferred from the TransantarcticMountains (TAM)
1347 micrometeorite collection. *Journal of Geophysical Research: Planets* **125**,
1348 e2019JE006241. https://doi.org/10.1029/2019JE006241.

1349 Taylor S., Lever J. H. and Harvey R. P. (2000) Numbers, types, and compositions of an
1350 unbiased collection of cosmic spherules. *Meteorit. Planet. Sci.* **35**, 651-666.
1351 https://doi.org/10.1111/j.1945-5100.2000.tb01450.x.

1352 Taylor S., Herzog G. F. and Delaney J. S. (2007) Crumbs from the crust of Vesta:
1353 Achondritic cosmic spherules from the South Pole water well. *Meteorit.Planet. Sci.*
1354 **42**, 223-233. https://doi.org/10.1111/j.1945-5100.2007.tb00229.x.

1355 Taylor S., Matrajt G. and Guan Y. (2012) Fine-grained precursors dominate the
1356 micrometeorite flux. *Meteorit. Planet. Sci.* **47**, 550-564. https://doi.org/10.1111/j.1945-
1357 5100.2011.01292.x.

1358 Toppani A., Libourel G., Engrand C. and Maurette M. (2001) Experimental simulation of
1359 atmospheric entry of micrometeorites. *Meteorit. Planet. Sci.* **36**, 1377-1396.
1360 https://doi.org/10.1111/j.1945-5100.2001.tb01831.x.

1361 Trappitsch R. and Leya I. (2013) Cosmogenic production rates and recoil loss effects in
1362 micrometeorites and interplanetary dust particles. *Meteorit. Planet. Sci.* **48**, 195-210.
1363 https://doi.org/10.1111/maps.12051.

1364 Trappitsch R. and Leya I. (2016) Production and recoil loss of cosmogenic nuclides in
1365 presolar grains. *Astrophy. J.* **823**, 12. https://doi.org/10.3847/0004-637X/823/1/12.

1366 Trieloff M., Kunz J., Clague D. A., Harrison D. and Allègre C. J. (2000) The nature of
1367 pristine noble gases in mantle plumes. *Science* **288**, 1036-1038.
1368 https://doi.org/10.1126/science.288.5468.1036.

1369 van Ginneken M., Folco L., Cordier C. and Rochette P. (2012) Chondritic micrometeorites
1370 from the Transantarctic Mountains. *Meteorit. Planet. Sci.* **47**, 228-247.
1371 https://doi.org/10.1111/j.1945-5100.2011.01322.x.

1372 Vogel N., Heber V. S., Baur H., Burnett D. S. and Wieler R. (2011) Argon, krypton, and
1373 xenon in the bulk solar wind as collected by the Genesis mission. *Geochim. Cosmochim.*
1374 *Acta*, **75**, 3057-3071. https://doi.org/10.1016/j.gca.2011.02.039.

1375 Vogt M., Hopp J., Gail H.-P., Ott U. and Trieloff M. (2019) Acquisition of terrestrial neon
1376 during accretion – A mixture of solar wind and planetary components. *Geochim.*
1377 *Cosmochim. Acta* **264**, 141-164. https://doi.org/10.1016/j.gca.2019.08.016.

1378 Wieler R. (2002a) Noble gases in the Solar System. In: *Noble Gases in Geochemistry and*
1379 *Cosmochemistry* (eds. D. Porcelli, C. J. Ballentine and R. Wieler). *Rev. Min. Geochem.*
1380 **47**, 21-70. https://doi.org/10.2138/rmg.2002.47.2.

1381 Wieler R. (2002b) Cosmic-ray-produced noble gases in meteorites. In: *Noble Gases in*
1382 *Geochemistry and Cosmochemistry* (eds. D. Porcelli, C. J. Ballentine and R. Wieler).
1383 *Rev. Min. Geochem*. **47**, 125-170. https://doi.org/10.2138/rmg.2002.47.5.

1384 Wieler R., Grimberg A. and Heber V. S. (2007) Consequences of the non-existence of the
1385 "SEP" component for noble gas geo-and cosmochemistry. *Chem. Geol.* **244**, 382-390.
1386 https://doi.org/10.1016/j.chemgeo.2007.06.026.

1387 Wyatt S. P. and Whipple F. L. (1950) The Poynting-Robertson effect on meteor orbits.
1388 *Astrophys. Journ.* **111**, 134-141. https://doi.org/ 10.1086/145244.

1389 Yabuta, H., Noguchi T., Itoh S., Nakamura T., Miyake A., Tsujimoto S., Ohashi N.,
1390 Sakamoto N., Hashiguchi M., Abe K.-i., Okubo A., Kilcoyne A. L. D., Tachibana S.,
1391 Okazaki R., Terada K., Ebihara M. and Nagahara H. (2017) Formation of an
1392 ultracarbonaceous Antarctic micrometeorite through minimal aqueous alteration in a
1393 small porous icy body. *Geochim. Cosmochim. Acta* **214**, 172-190.
1394 https://doi.org/10.1016/j.gca.2017.06.047.